QUALITY CONTROL

Identification of a quality-control factor that monitors failures during proteasome assembly

Eszter Zavodszky[1], Sew-Yeu Peak-Chew[1], Szymon Juszkiewicz[1], Ana J. Narvaez[2]†, Ramanujan S. Hegde[1]*

In eukaryotic cells, half of all proteins function as subunits within multiprotein complexes. Imbalanced synthesis of subunits leads to unassembled intermediates that must be degraded to minimize cellular toxicity. Here, we found that excess PSMC5, a subunit of the proteasome base, was targeted for degradation by the HERC1 ubiquitin ligase in mammalian cells. HERC1 identified unassembled PSMC5 by its cognate assembly chaperone PAAF1. Because PAAF1 only dissociates after assembly, HERC1 could also engage later assembly intermediates such as the PSMC4-PSMC5-PAAF1 complex. A missense mutant of HERC1 that causes neurodegeneration in mice was impaired in the recognition and ubiquitination of the PSMC5-PAAF1 complex. Thus, proteasome assembly factors can serve as adaptors for ubiquitin ligases to facilitate elimination of unassembled intermediates and maintain protein homeostasis.

Many of the cell's multisubunit complexes, such as ribosomes and proteasomes, are exceptionally abundant and contain a large number of subunits. Their maturation can involve dozens or more assembly factors that participate in a multistep pathway (*1*–*3*). The different subunits cannot be produced at a precise desired stoichiometry owing to the inherent noisiness of transcription and translation (*4*, *5*). For highly abundant complexes, even subtle imbalances in subunit synthesis (*6*) can produce an appreciable number of assembly intermediates awaiting the next component. Furthermore, cellular stress and various disease states, most notably cancer, can exaggerate subunit imbalances because of altered or dysregulated gene expression (*6*–*8*). As exemplified by the thalassemias (*9*) or aneuploidy (*10*–*13*), excessive or chronic subunit imbalance can have detrimental gain-of-function consequences. How cells detect stalled orphaned assembly intermediates for selective elimination is not well understood.

Identification of degraded candidate orphan proteins

To find prominent orphan proteins caused by imbalanced gene expression, we identified rapidly degraded proteins in the aneuploid breast cancer cell line MCF7. We pulse-labeled nascent proteins for 1 hour with the methionine analog azido-homoalanine (AHA) followed by a chase with methionine for up to 8 hours. The AHA-containing proteins across all time points were captured by click chemistry (*14*) and analyzed by quantitative proteomics (Fig. 1A, fig. S1, and table S1). Focusing on the cell's ~450 most highly translated proteins (from 2262 total identified proteins), we found that a minor subset of nascent proteins decreased abruptly in the first hour (Fig. 1B). Notably, 14 of the top 15 such proteins were subunits of multiprotein complexes.

Only a subset of subunits that comprise the proteasome, chaperonin, and ribosome displayed nonexponential degradation, where a proportion of the protein was degraded rapidly and the remainder was comparatively stable (Fig. 1, B and C, and fig. S2). By contrast, degradation of proteins that were not stable subunits of complexes, or the loss of proteins because of secretion, followed exponential decay (fig. S2C). These findings could not be explained by AHA-induced protein misfolding (tables S2 and S3) (*15*) or imbalanced subunit production caused by methionine starvation during AHA labeling (table S4) (*16*).

Instead, the collection of mRNAs for degraded proteins was more highly increased in MCF7 cells than in any of 10 other similar breast cancer cell lines (Fig. 1D) (*17*). The degree of increase for these mRNAs was also greater than that for the set of mRNAs coding for the stable proteins (Fig. 1E). The mRNAs for degraded subunits of the proteasome and ribosome were overrepresented by around 1.5- to 2-fold in MCF7 cells, but not other breast cancer cell lines, relative to the mRNAs for the stable subunits of the respective complex (Fig. 1F and fig. S3). This degree of excess mRNA roughly matched the ~30 to 50% of their encoded proteins that were rapidly degraded. Thus, subunits of multiprotein complexes are major targets for quality control in cancer cells because a population of these proteins evidently become orphaned when they are expressed inappropriately at higher levels than their assembly partners.

HERC1 interacts with and ubiquitinates nascent PSMC5

To identify the quality-control pathway(s) that facilitate orphan degradation, we analyzed individual subunits of four diverse multiprotein complexes identified as orphans in our proteomics analysis of MCF7 cells. Each epitope-tagged subunit was synthesized in a reticulocyte-based cell-free translation extract with the aim of finding at least one whose recognition for quality control was recapitulated in this system. Two subunits, PSMC5 of the proteasome and CCT3 of the cytosolic chaperonin, were ubiquitinated (Fig. 2A). Both complexes are abundant in reticulocytes (*18*, *19*), explaining why factors needed for their quality control are present in this system. Conversely, subunits of the spliceosome and myosin, which do not have an appreciable role in reticulocyte biology, were poorly recognized.

Focusing on newly made PSMC5, we observed that its immunoprecipitation under nondenaturing conditions coprecipitated ubiquitin ligase activity (fig. S4A). Large-scale affinity purification of nascent PSMC5 followed by mass spectrometry identified the HECT-domain protein HERC1 as the sole E3 ubiquitin ligase (Fig. 2B and table S5). This interaction was verified by coimmunoprecipitation and immunoblotting (fig. S4B). Furthermore, HERC1 cofractionated selectively with the ubiquitinated subpopulation of PSMC5 when separated by size by sedimentation through a sucrose gradient (Fig. 2C).

The other interaction partners of nascent PSMC5 suggested that it was engaged in a heterogeneous set of assembly intermediates consistent with PSMC5's broad distribution across the sucrose gradient. The most abundant interaction partner was PSMC5's dedicated chaperone PAAF1 (fig. S4B) (*20*–*23*). Other subunits of the 19*S* base were copurified at lower levels, consistent with partial assembly of PSMC5 with endogenous base subunits present in the lysate (table S5). Assembly beyond this step was evidently less efficient, with incomplete recovery of 19*S* lid subunits and essentially no recovery of 20*S* core subunits.

Engagement of PSMC5 with the 20*S* core would be impaired by the C-terminal epitope tag, thereby ensuring that nearly all nascent PSMC5 would stall at earlier assembly intermediates. Based on the staining intensity of the products (Fig. 2B) and sucrose gradient distribution (Fig. 2C), the most abundant complex was the PSMC5-PAAF1 assembly intermediate. Thus, this unassembled product might be at least one quality-control target of HERC1.

PSMC5 synthesized in a translation system reconstituted from purified recombinant *Escherichia coli* translation factors (known as the PURE system) was entirely insoluble unless a chaperone, such as recombinant PAAF1, was included during translation (fig. S5A). The PSMC5-PAAF1 heterodimer from the peak fractions of the gradient could be ubiquitinated by full-length recombinant HERC1 at physiologic concentrations, but not by a C-terminal domain that retains full E3 ligase

[1]MRC Laboratory of Molecular Biology, Cambridge, UK. [2]Discovery Sciences, AstraZeneca, Cambridge, UK.
*Corresponding author. Email: rhegde@mrc-lmb.cam.ac.uk
†Present address: Moderna Therapeutics, Cambridge, MA, USA.

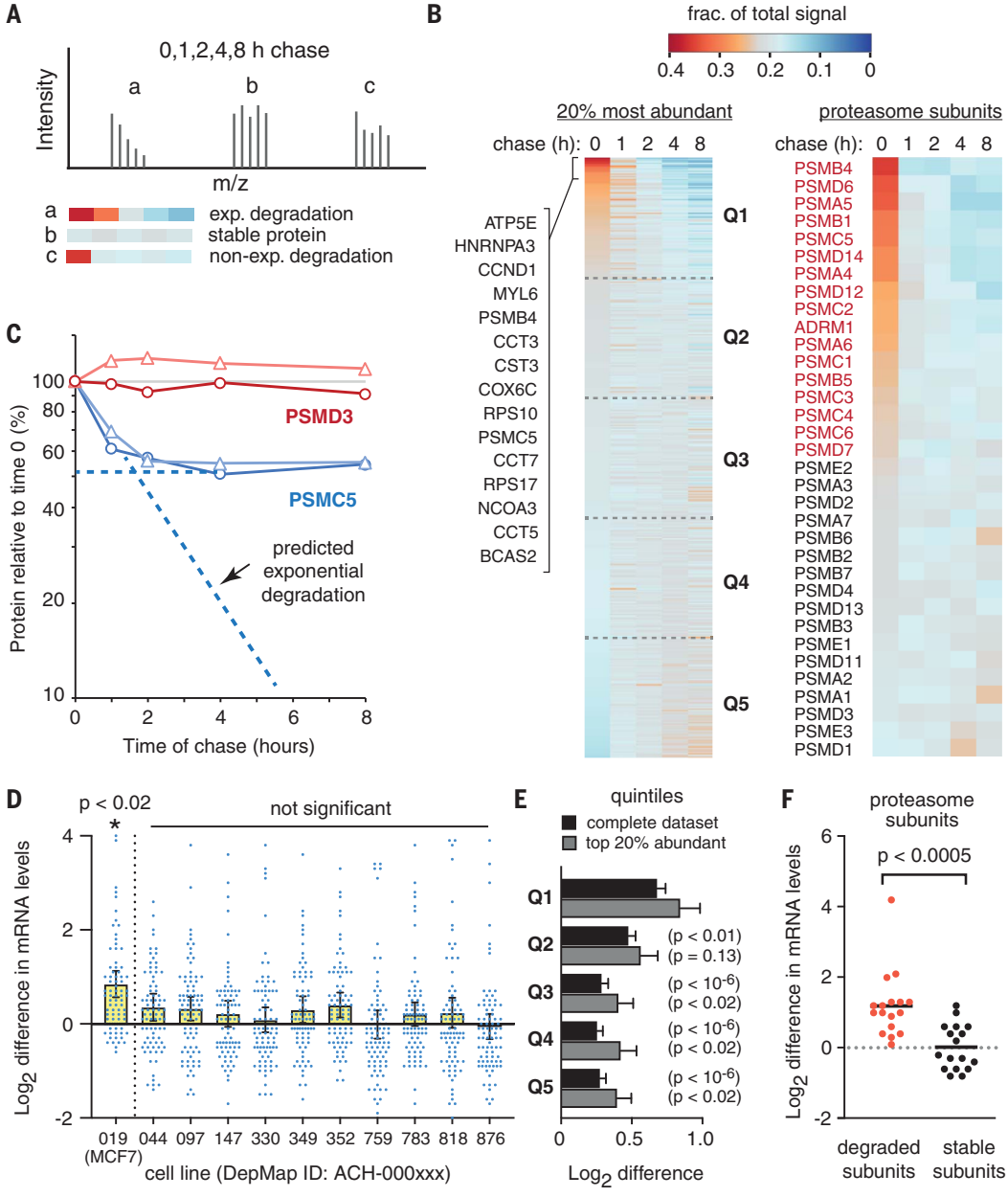

Fig. 1. Identification of rapidly degraded candidate orphans. (**A**) Schematic of how tandem mass tag mass spectrometry data from a pulse chase is displayed as a heat map to visualize a protein's change over time. The relative proportion of the total signal at each time point is displayed in the heat map (red is high; blue is low) for each hypothetical peptide's spectra. exp., exponential. (**B**) Heat maps as in (A) are shown for the 20% most abundant proteins (left) and for subunits of the proteasome (right). Identities of the first 15 proteins of the left heat map are indicated. Each quintile is indicated (Q1 to Q5). (**C**) Data from (B) showing examples of nonexponential degradation (PSMC5) and a stable protein (PSMD3). Each of two replicates is shown in different shades. (**D**) Individual mRNA levels for quintile-1 proteins from (B) (together with their means ± 95% confidence intervals) are shown for 11 cell lines derived from HER2-negative and estrogen receptor–positive breast cancers. Each mRNA level is expressed as the $\log_2$ difference from that mRNA's average level across all 1379 cell lines in the DepMap database. Only MCF7 cells showed a significant ($p < 0.02$) increase of this set of mRNAs, which was also significantly different ($p < 0.02$) from the levels in all the other breast cancer cell lines. (**E**) Plot as in (D) comparing the mRNA levels (means ± SEM) for Q1 through Q5 in MCF7 cells. p values for a two-tailed Student's t test comparison to Q1 are indicated. (**F**) Plot as in (D) for the degraded and stable subunits of the proteasome shown in (B), using the same color-coding as in (B). The black horizontal lines indicate the mean.

activity (Fig. 2D and fig. S5B). Thus, HERC1 can recognize the unassembled PSMC5-PAAF1 complex and ubiquitinate PSMC5.

HERC1 facilitates degradation of PSMC5 in cells

Pulse-chase experiments using ^{35}S-methionine showed that roughly half of newly synthesized PSMC5 was degraded shortly after synthesis in MCF7 cells (fig. S6A). PSMC5 degradation was blunted in cells knocked out for HERC1 (fig. S6B). Proteomic analysis of nascent proteins synthesized during 1 hour in untreated versus HERC1 knockdown (KD) cells revealed that PSMC5 was overrepresented (~1.4-fold) in KD cells (Fig. 2E and table S6). Relatively few other proteins were overrepresented similarly, indicating that HERC1 does not generally influence protein synthesis or degradation. For example, chaperonin subunits, ribosomal proteins, and most subunits of the proteasome were unaffected (Fig. 2E). By contrast, five of six adenosine triphosphatase (ATPase) subunits (including PSMC5) of the 19*S* proteasome base were overrepresented in the KD sample, suggesting that this class of proteins was selectively influenced by HERC1.

Although the burden of surplus PSMC5 and other subunits is exaggerated in MCF7 cells, ~10 to 20% imbalanced production can occur in normal cells owing to gene expression noise (*4*, *5*). Indeed, 19*S* ATPase subunits were modestly (by ~21%) but significantly stabilized upon HERC1 KD in the noncancer breast epithelial cell line MCF10a (fig. S7 and table S7). Subunits of the cytosolic chaperonin (CCTs), which are not targets for HERC1, were not changed in HERC1 KD cells. Thus, the problem of subunit imbalance, although enhanced by genomic dysregulation in cancer cells, is nonetheless appreciable in noncancer cells.

These proteomic observations were examined in focused assays using fluorescent protein reporters. Reporter translation produces two fluorescent proteins: green fluorescent protein (GFP) that is fused to a protein of interest and red fluorescent protein (RFP). The GFP:RFP ratio provides a quantitative assessment of any changes to the GFP-tagged protein's stability (*24*). Overexpressed N-terminally–tagged PSMC5 was mostly degraded but was

stabilized by KD or knockout (KO) of HERC1 in MCF7 cells (Fig. 2F and fig. S8).

Furthermore, degradation of excess subunits of other complexes or a subunit of the 20*S* proteasome core was not affected by HERC1 KD (Fig. 2F and fig. S9A). Surprisingly, other 19*S* ATPase ring members that were affected by HERC1 KD in the proteomics experiment were neither degraded as effectively as PSMC5 nor affected strongly by HERC1 KO when tested by exogenous overexpression in the reporter assay (Fig. 2F and fig.

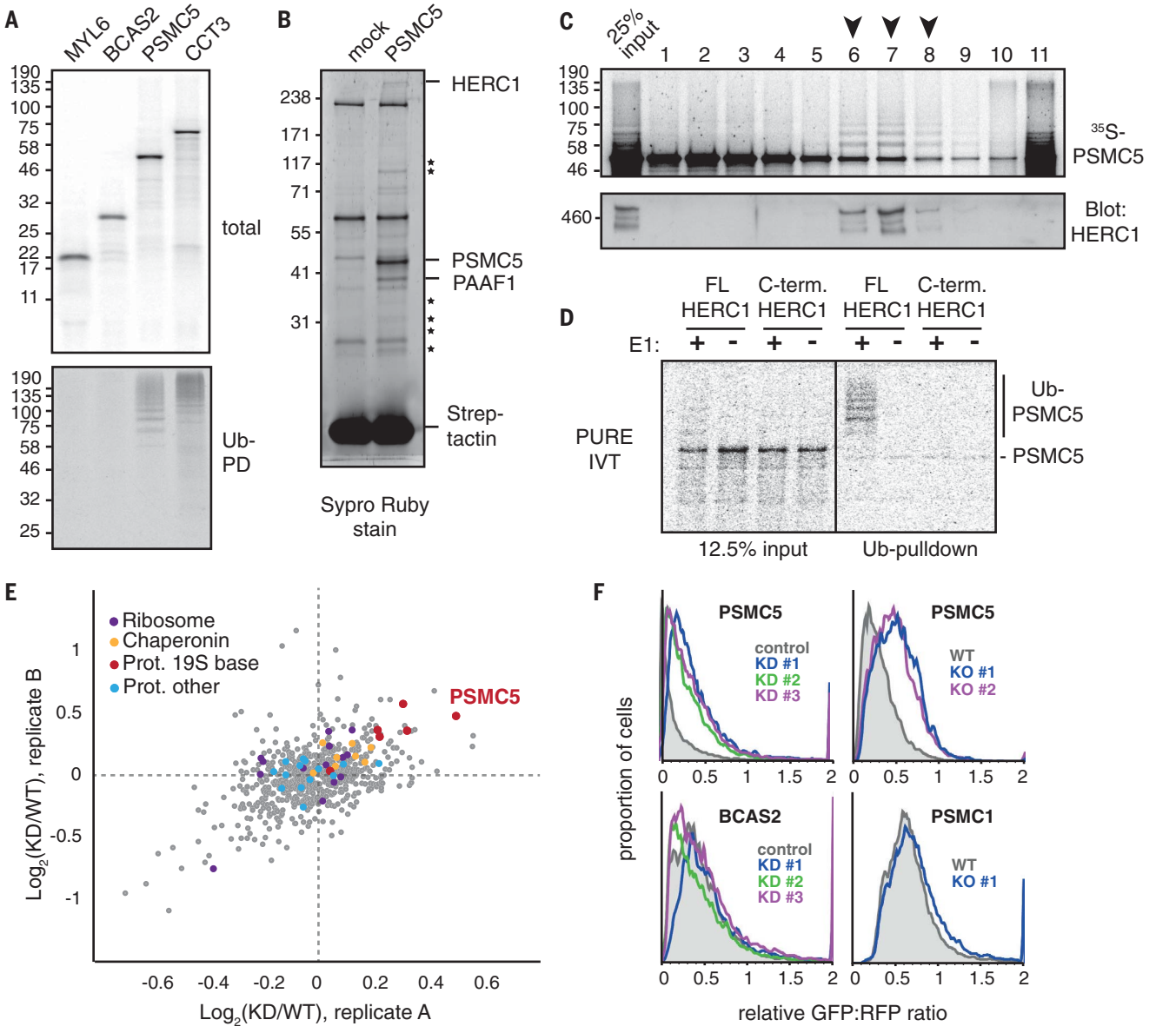

Fig. 2. HERC1 mediates nascent PSMC5 degradation. (**A**) Subunits of four different multimeric complexes were translated in rabbit reticulocyte lysate (RRL) containing ^{35}S-methionine and His-tagged ubiquitin (Ub). PD, pull down. Ubiquitinated translation products were isolated by Ni-nitrilotriacetic acid (Ni-NTA) pull down under denaturing conditions. (**B**) PSMC5 containing a twin-Strep tag (TST) was translated in RRL and affinity-purified under native conditions using immobilized Streptactin, and the products were visualized by SYPRO Ruby stain. Mock indicates a parallel reaction lacking mRNA. The indicated PSMC5-specific interaction partners were identified by mass spectrometry, with stars denoting other 19*S* subunits of the proteasome. (**C**) ^{35}S-methionine–labeled PSMC5 translated in in RRL was separated on a 5 to 25% sucrose gradient. Fractions were analyzed by autoradiography for PSMC5 and by immunoblot for HERC1. Arrows indicate fractions where ubiquitinated PSMC5 cofractionates with HERC1. On this gradient, ~300-kD protein typically migrates in fractions three to five, and a ~500-kD protein in fractions five to seven. (**D**) ^{35}S-methionine–labeled PSMC5 in complex with PAAF1 was produced by translation in the PURE system (see fig. S5A). The complex was mixed with E1, E2, His-Ub, adenosine triphosphate (ATP), and either full-length (FL) or truncated recombinant HERC1 (see fig. S5B). Ubiquitinated products were isolated by Ni-NTA pull down under denaturing conditions and visualized by autoradiography. IVT, in vitro translation. (**E**) MCF7 cells were pretreated with nontargeting (WT) or HERC1-targeting (KD) small interfering RNAs (siRNAs) and metabolically labeled for 1 hour with AHA. The labeled proteins were selectively recovered using click chemistry, and the recovered proteins were analyzed by quantitative mass spectrometry. The top 20% most abundant proteins from two biological replicates are plotted by the KD/WT ratio, with subunits of the proteasome, ribosome, and chaperonin highlighted. (**F**) Flow cytometry analysis of GFP-tagged reporter proteins compared with an internal RFP control. HERC1 was knocked down by three separate siRNAs (KD) or knocked out using CRISPR (KO).

S9B). This suggested that the effect of HERC1 on non-PSMC5 base subunits could be indirect, an idea consistent with relatively poor interaction of most of these subunits with HERC1 in vitro despite their considerable sequence and structural homology to each other (fig. S10A).

PAAF1 is required for recognition of PSMC5 by HERC1

To understand why overexpressed PSMC5, but not other base subunits, was degraded via HERC1, we investigated the mechanism of HERC1 target selection. Although each subunit of the 19*S* ATPase ring is similar, their C-terminal domains engage different assembly factors (*20*–*23*, *25*). Recognizing that our reconstituted ubiquitination experiment (Fig. 2D) used the PSMC5-PAAF1 complex as a substrate (fig. S5), we tested whether PAAF1 plays a role in HERC1 recognition. Indeed, in vitro–translated PSMC5 lacking the C-terminal domain (PSMC5ΔC) did not bind PAAF1, showed reduced HERC1 binding, and showed reduced ubiquitination compared with full-length PSMC5 (Fig. 3, A and B).

Although overexpressed PSMC5ΔC was degraded in MCF7 cells, its degradation did not depend on HERC1 (Fig. 3C). This suggested that HERC1 either recognizes the C terminus, recognizes PAAF1, or that non-native interaction partners of PSMC5ΔC (fig. S10B) obscure HERC1 access. To distinguish between these possibilities, we tested PSMC5 ubiquitination when it is complexed with another 19*S* assembly chaperone (PSMD10), is complexed with the nonphysiologic chaperone-like protein calmodulin (*26*), or is uncomplexed with any factor. PSMC10 ordinarily chaperones the C-terminal domain of PSMC4 but can engage PSMC5 in the purified translation reaction owing to the homology between their C-terminal domains. Calmodulin, by contrast, has broad Ca^{2+}-dependent binding activity. Both proteins precluded nascent PSMC5 aggregation

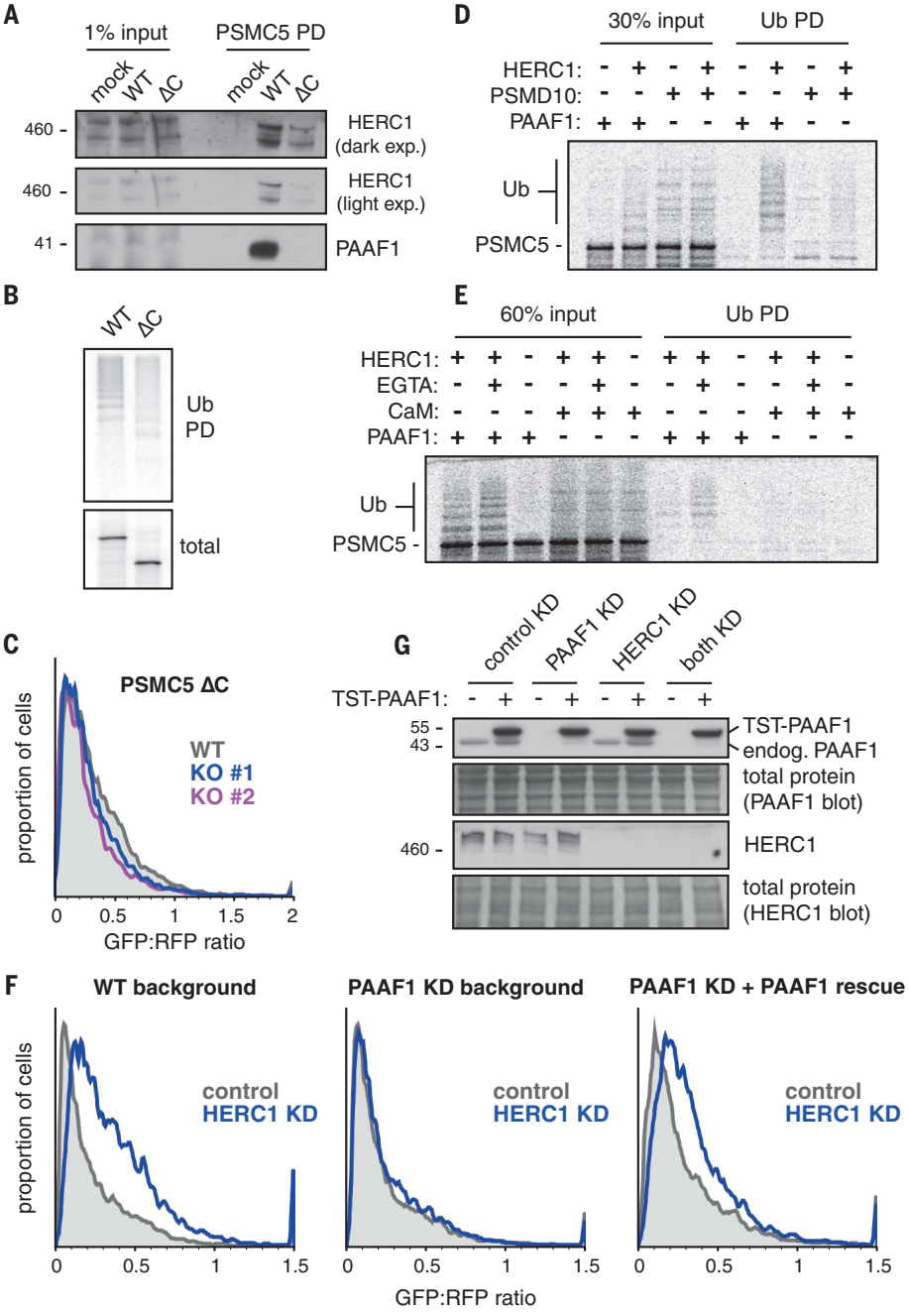

Fig. 3. The assembly chaperone PAAF1 participates in HERC1 target selection. (**A**) Full-length PSMC5 (WT) and PSMC5 lacking its C-terminal 86 residues (ΔC) were translated in RRL and affinity-purified under native conditions using a C-terminal TST. The input and purified samples were blotted for HERC1 and PAAF1. SYPRO-Ruby staining (fig. S10B) was used to verify equal recovery of the translation products. (**B**) Full-length and truncated PSMC5 were translated in RRL in the presence of ^{35}S-methionine and His-tagged ubiquitin (Ub). Ubiquitinated products were isolated by Ni-NTA pull down. (**C**) Flow cytometry analysis of GFP-tagged C-terminally truncated PSMC5 in WT and HERC1 KO MCF7 cells. (**D**) ^{35}S-methionine–labeled PSMC5 in complex with PAAF1 or PSMD10 was prepared by translation in the PURE system. The complexes were mixed with E1, E2, His-Ub, ATP, and full-length recombinant HERC1. Ubiquitinated products were isolated by Ni-NTA pull down under denaturing conditions. (**E**) ^{35}S-methionine–labeled PSMC5 in complex with PAAF1 or calmodulin (CaM) was prepared and mixed with ubiquitination components, as in (D). Where indicated, EGTA was used to dissociate CaM from PSMC5. Ubiquitinated products were isolated by Ni-NTA pull down under denaturing conditions. (**F**) Flow cytometry analysis of GFP-tagged PSMC5 in MCF7 cells. HERC1 and PAAF1 were knocked down separately or simultaneously by single siRNA oligonucleotides. TST-PAAF1 with siRNA-resistant silent mutations was reintroduced where indicated (PAAF1 rescue). (**G**) KD of endogenous PAAF1 and HERC1, as well as rescue with TST-PAAF1, was verified by immunoblot for the experiment in (F).

sufficiently well in the PURE system to provide substrate complexes for HERC1 ubiquitination assays.

HERC1 did not effectively ubiquitinate either the PSMC5-PSMD10 complex or the PSMC5-calmodulin complex (Fig. 3, D and E). EGTA-mediated release of calmodulin to fully expose PSMC5 to HERC1 also did not permit ubiquitination. Thus, neither uncomplexed PSMC5 nor PSMC5 complexed with PSMD10 or calmodulin was recognized by HERC1, illustrating a crucial role for PAAF1 in recognition. Indeed, HERC1 depletion failed to stabilize PSMC5 in cells depleted of PAAF1 (Fig. 3F). Efficient PSMC5 recognition by HERC1 therefore relies on PSMC5's chaperone PAAF1. PSMC5 produced in the absence of PAAF1 is presumably misfolded (consistent with its aggregation in the PURE system), triggering PSMC5 degradation by a HERC1-independent pathway. This further indicates that HERC1 is not simply recognizing PSMC5 misfolding but rather is recognizing a PAAF1-containing putative assembly intermediate.

HERC1 interacts with a PSMC4-containing assembly intermediate

PAAF1 remains bound to the C-terminal domain of PSMC5 throughout its assembly with other ATPase subunits of the 19*S* base, dissociating concomitant with C-terminal insertion into the 20*S* core particle (*21*, *23*). Hence, assembly intermediates downstream of the initial PSMC5-PAAF1 complex are potential targets for HERC1, possibly explaining why other base subunits are affected by HERC1 KD in the context of PSMC5 excess. To test this idea, we determined if the PSMC5-PSMC4 assembly intermediate is targeted by HERC1 using retained PAAF1.

In vitro–translated PSMC4 interacted equally well with coexpressed PSMC5 and PSMC5ΔC (Fig. 4A, top), verifying that each nascent subunit is assembly-competent. Affinity purification of PSMC4 coprecipitated PAAF1 and HERC1 only from PSMC5-containing reactions, but not from reactions containing PSMC5ΔC or lacking PSMC5 (Fig. 4A, bottom). Thus, PSMC4 associates with HERC1 through the PSMC5-PAAF1 complex. In accordance with HERC1 recruitment, the PSMC5-PSMC4 intermediate remains vulnerable to ubiquitination (fig. S11). Thus, assembly of PSMC5 with PSMC4 does not protect PSMC5 from ubiquitination, presumably because retained PAAF1 is still able to recruit HERC1 to the complex.

Although overexpressed fluorescent PSMC4 is mostly degraded independently of HERC1, coexpression with nonfluorescent PSMC5 imparts partial HERC1 dependence to PSMC4 degradation (Fig. 4B). This provides in vivo support for HERC1 targeting PSMC4 by recognition of the associated PSMC5-PAAF1 complex. These observations provide an explanation for partial PSMC4 stabilization in MCF7 cells knocked down for HERC1 (Fig. 2E). Although we have not examined other assembly intermediates, it is plausible that later PAAF1-containing complexes are also potential targets for HERC1.

Why does HERC1 not interfere with normal assembly? One model is kinetic competition (*27*, *28*), with assembly occurring faster than HERC1 recognition. This mechanism is plausible because HERC1 is ~10-fold less abundant than PAAF1 (*29*, *30*). Boosting HERC1 levels using CRISPR activation (*31*) of the endogenous *HERC1* promoter led to promiscuous degradation of endogenous nascent PSMC5 and PSMC4 (fig. S12), supporting a competition-based mechanism.

Disease-causing HERC1 mutant is deficient in PSMC5 recognition

Coimmunoprecipitation experiments using a series of domain deletion constructs expressed in cultured cells showed that the first RCC1-like domain (RLD1) in HERC1 is important for interaction with PSMC5 (fig. S13). This finding was illuminating because the recessive neurodegeneration-causing *tambaleante* allele in mouse was mapped to a Gly^{483}→Glu (G483E) missense mutation in RLD1 of HERC1. Biochemical analysis of purified HERC1 variants (fig. S14) showed that the ΔRLD1 deletion mutant and G483E point mutant were impaired in their interaction with nascent PSMC5, whereas other deletion mutants were not (Fig. 5A and fig. S15A).

Ubiquitination assays using the PSMC5-PAAF1 complex produced in the PURE system showed a marked reduction of PSMC5 ubiquitination by the ΔRLD1 and G483E mutants (Fig. 5B and fig. S15B) despite no impairment of autoubiquitination (fig. S15C). This suggests that G483E is specifically deficient in interaction with and ubiquitination of PSMC5. This mutant is expressed normally in mouse (*32*) and cultured cells with comparable biochemical behavior as the wild-type (WT) protein (fig. S15, D and E), illustrating that the mutant protein is not grossly misfolded or eliminated by cellular quality control. These results suggest that a deficiency in HERC1-mediated quality control contributes to the disease phenotype of *tambaleante* mice. Consistent with this idea, the impaired cell types in mice are those that most rely on effective proteostasis (*33*), especially Purkinje cells, which are frequently lost with perturbed proteostasis (*34*–*36*).

Conclusions and perspective

Unassembled subunits have long been appreciated to be quality-control targets for one of

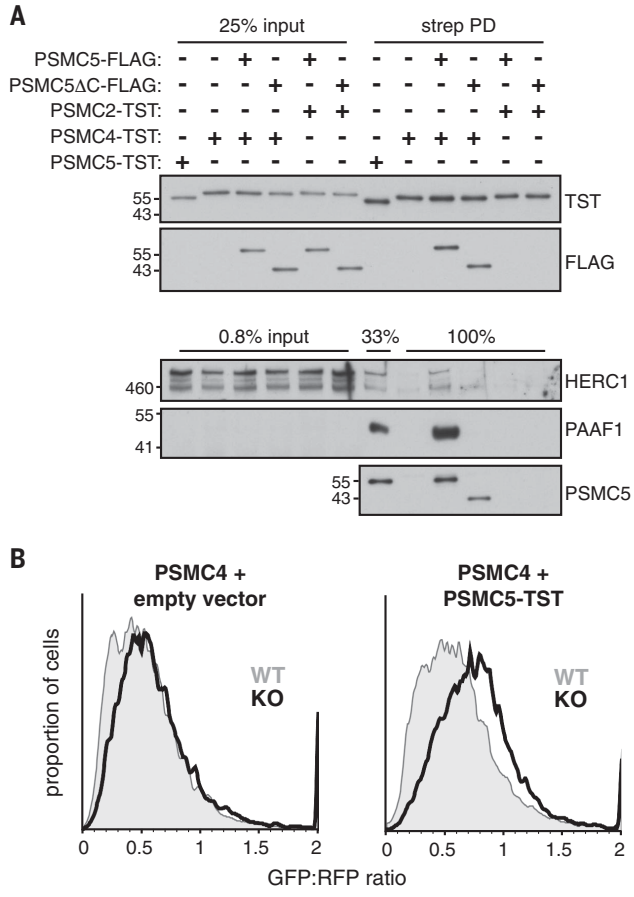

Fig. 4. HERC1 recognizes multiple assembly intermediates using PAAF1. (**A**) FLAG-tagged full-length or C-terminally truncated (ΔC) PSMC5 was cotranslated with a twin-Strep-tagged partner ATPase (PSMC4) or distal ring member (PSMC2) in RRL. Complexes were affinity purified using the TST and blotted for TST, FLAG, HERC1, PAAF1, and PSMC5 as indicated. TST-PSMC5 was translated and purified directly as a positive control. Reactions containing only one ring member included mRNA for an irrelevant protein (the cytosolic domain of Sec61β) to ensure equal rates of synthesis. The relative amounts of the different samples loaded for the two sets of blots are indicated. (**B**) Flow cytometry analysis of GFP-tagged PSMC4 in WT and HERC1 KO MCF7 cells, with and without cotransfection of nonfluorescent PSMC5.

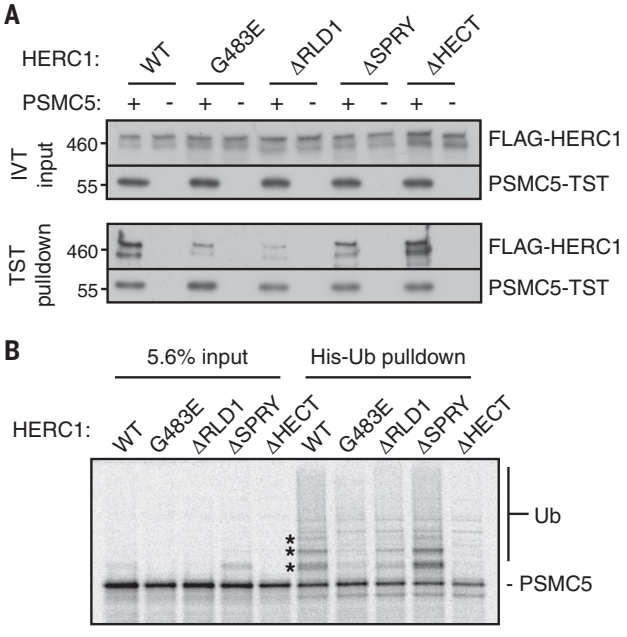

Fig. 5. Disease-causing HERC1 mutant is deficient in PSMC5 recognition and ubiquitination. (**A**) Recombinant purified FLAG-tagged HERC1 proteins (see fig. S14) were added at 2 nM to RRL in vitro translation reactions with or without mRNA for twin-Strep-tagged PSMC5. PSMC5-TST was affinity purified under native conditions using Strep-tactin, and inputs and elutions were visualized by immunoblotting. (**B**) ^{35}S-methionine–labeled PSMC5 in complex with PAAF1 was produced by translation in the PURE system (as in fig. S5A). The complex was mixed with E1, E2, His-Ub, ATP, and 8 nM of WT or mutant HERC1. Ubiquitinated products were enriched by Ni-NTA pull down under denaturing conditions. The input and ubiquitin pull-down samples were visualized by autoradiography. The positions of mono-, di-, and tri-ubiquitinated PSMC5 are indicated with asterisks (also visible faintly in the input sample).

two reasons: either they misfold in the absence of assembly or the exposed assembly interface is recognized by quality-control factors (*37*–*40*). In both cases, exposed hydrophobic surfaces are thought to be the target for quality control. Our findings reveal a qualitatively different mechanism: Delayed assembly cues ubiquitin ligase recruitment using the associated assembly factor. A major advantage for the cell of such a kinetic competition mechanism is that recognition does not depend on potentially toxic misfolding or aggregation. Instead, a simple delay would be sufficient to trigger elimination of otherwise normal intermediates. By using an assembly factor to identify incomplete products, a ubiquitin ligase can potentially recognize multiple intermediates along the assembly pathway.

HERC1 is both widely expressed and widely conserved (*41*, *42*). Loss of HERC1 function in mice and humans leads to neurological defects (*32*, *43*–*46*) associated with deficient proteostasis (*33*). Our finding that a neurodegeneration-causing missense mutation is strongly impaired in PSMC5 ubiquitination in a purified system implicates this quality-control pathway in maintaining proteostasis in vivo. More generally, the insights provided here should motivate systematic searches for assembly factor–dependent ubiquitin ligases that eliminate stalled intermediates of other major cellular complexes. Because orphan proteins and intermediates are especially prominent in cancer cells with aberrant gene expression, mechanisms to eliminate these products may be important for their rapid growth. Intriguingly, HERC1 is up-regulated in various cancer cell lines and tumors (*42*), and its overexpression can provide a selective advantage to tumor growth and metastasis in mouse (*47*). RNA sequencing of a wide range of cancer-derived cells (*17*) indicates that different populations of orphans feature in different tumors. Thus, identifying the quality-control pathways for other abundant orphans using the approaches defined here may provide useful therapeutic targets.

REFERENCES AND NOTES

1. K. E. Bohnsack, M. T. Bohnsack, *EMBO J.* **38**, e100278 (2019).
2. S. Klinge, J. L. Woolford Jr., *Nat. Rev. Mol. Cell Biol.* **20**, 116–131 (2019).
3. A. Rousseau, A. Bertolotti, *Nat. Rev. Mol. Cell Biol.* **19**, 697–712 (2018).
4. J. M. Raser, E. K. O'Shea, *Science* **309**, 2010–2013 (2005).
5. B. Munsky, G. Neuert, A. van Oudenaarden, *Science* **336**, 183–187 (2012).
6. J. W. Harper, E. J. Bennett, *Nature* **537**, 328–338 (2016).
7. Y.-C. Tang, A. Amon, *Cell* **152**, 394–405 (2013).
8. D. Hanahan, R. A. Weinberg, *Cell* **144**, 646–674 (2011).
9. R. Origa, *Genet. Med.* **19**, 609–619 (2017).
10. C. M. Brennan *et al.*, *Genes Dev.* **33**, 1031–1047 (2019).
11. N. Dephoure *et al.*, *eLife* **3**, e03023 (2014).
12. E. M. Torres *et al.*, *Science* **317**, 916–924 (2007).
13. B. R. Williams *et al.*, *Science* **322**, 703–709 (2008).
14. D. C. Dieterich, A. J. Link, J. Graumann, D. A. Tirrell, E. M. Schuman, *Proc. Natl. Acad. Sci. U.S.A.* **103**, 9482–9487 (2006).
15. E. McShane *et al.*, *Cell* **167**, 803–815.e21 (2016).
16. C. C. Thoreen *et al.*, *Nature* **485**, 109–113 (2012).
17. M. Ghandi *et al.*, *Nature* **569**, 503–508 (2019).
18. N. J. Cowan, *Methods Enzymol.* **290**, 230–241 (1998).
19. J. Driscoll, A. L. Goldberg, *J. Biol. Chem.* **265**, 4789–4792 (1990).
20. M. Funakoshi, R. J. Tomko Jr., H. Kobayashi, M. Hochstrasser, *Cell* **137**, 887–899 (2009).
21. T. Kaneko *et al.*, *Cell* **137**, 914–925 (2009).
22. J. Roelofs *et al.*, *Nature* **459**, 861–865 (2009).
23. Y. Saeki, A. Toh-E, T. Kudo, H. Kawamura, K. Tanaka, *Cell* **137**, 900–913 (2009).
24. E. Itakura *et al.*, *Mol. Cell* **63**, 21–33 (2016).
25. S. Park *et al.*, *Nature* **459**, 866–870 (2009).
26. S. Shao, R. S. Hegde, *Cell* **147**, 1576–1588 (2011).
27. S. Shao, R. S. Hegde, *Trends Biochem. Sci.* **41**, 124–137 (2016).
28. S. Wickner, M. R. Maurizi, S. Gottesman, *Science* **286**, 1888–1893 (1999).
29. D. N. Itzhak, S. Tyanova, J. Cox, G. H. Borner, *eLife* **5**, e16950 (2016).
30. N. A. Kulak, G. Pichler, I. Paron, N. Nagaraj, M. Mann, *Nat. Methods* **11**, 319–324 (2014).
31. S. Konermann *et al.*, *Nature* **517**, 583–588 (2015).
32. T. Mashimo *et al.*, *PLOS Genet.* **5**, e1000784 (2009).
33. R. Ruiz, E. M. Pérez-Villegas, S. Bachiller, J. L. Rosa, J. A. Armengol, *Front. Neuroanat.* **10**, 42 (2016).
34. T. Hara *et al.*, *Nature* **441**, 885–889 (2006).
35. L. Zhao, C. Longo-Guess, B. S. Harris, J.-W. Lee, S. L. Ackerman, *Nat. Genet.* **37**, 974–979 (2005).
36. J. W. Lee *et al.*, *Nature* **443**, 50–55 (2006).
37. A. Shemorry, C.-S. Hwang, A. Varshavsky, *Mol. Cell* **50**, 540–551 (2013).
38. M.-K. Sung *et al.*, *eLife* **5**, e19105 (2016).
39. Y. Xu, D. E. Anderson, Y. Ye, *Cell Discov.* **2**, 16040 (2016).
40. K. Yanagitani, S. Juszkiewicz, R. S. Hegde, *Science* **357**, 472–475 (2017).
41. J. García-Cano, A. Martinez-Martinez, J. Sala-Gaston, L. Pedrazza, J. L. Rosa, *Front. Physiol.* **10**, 1014 (2019).
42. J. L. Rosa, R. P. Casaroli-Marano, A. J. Buckler, S. Vilaró, M. Barbacid, *EMBO J.* **15**, 4262–4273 (1996).
43. S. Aggarwal, A. D. Bhowmik, V. L. Ramprasad, S. Murugan, A. Dalal, *Am. J. Med. Genet. A.* **170**, 1868–1873 (2016).
44. L. S. Nguyen *et al.*, *Eur. J. Hum. Genet.* **24**, 455–458 (2016).
45. O. Ortega-Recalde *et al.*, *Clin. Genet.* **88**, e1–e3 (2015).
46. G. E. Utine *et al.*, *Eur. J. Med. Genet.* **60**, 279–283 (2017).
47. O. Fasano, D. Birnbaum, L. Edlund, J. Fogh, M. Wigler, *Mol. Cell. Biol.* **4**, 1695–1705 (1984).

ACKNOWLEDGMENTS

We thank members of the Hegde lab for productive discussions and comments on this manuscript; L. Figueiredo for help with heatmaps; M. Daly and F. Zhang for help with flow cytometry; and M. Kivlen for preparation of the PURE translation system. **Funding:** Funding was provided by UK Medical Research Council grant MC_ UP_A022_1007 (R.S.H.) and LMB-AZ BlueSky project BSF27 (A.J.N. and R.S.H.). **Author contributions:** E.Z. performed nearly all of the experiments. S.-Y.P.-C. performed mass spectrometry and contributed to its analysis. S.J. helped with mapping the substrate-binding domains of HERC1. E.Z., A.J.N., and R.S.H. conceived the project. E.Z. and R.S.H. wrote the manuscript. A.J.N. and R.S.H. provided project supervision. **Competing interests:** The authors declare that they have no competing interests. **Data and materials availability:** All data are available in the main text or the supplementary materials. Reagents used in this study are available from R.S.H. upon request.

SUPPLEMENTARY MATERIALS

science.sciencemag.org/content/373/6558/998/suppl/DC1
Materials and Methods
Figs. S1 to S15
Tables S1 to S7
References (*48*–*53*)
MDAR Reproducibility Checklist

View/request a protocol for this paper from *Bio-protocol*.

6 May 2020; resubmitted 22 June 2021
Accepted 15 July 2021
10.1126/science.abc6500

Science
AAAS

Supplementary Materials for

Identification of a quality-control factor that monitors failures during proteasome assembly

Eszter Zavodszky *et al.*

Corresponding author: Ramanujan S. Hegde, rhegde@mrc-lmb.cam.ac.uk

Science **373**, 998 (2021)
DOI: 10.1126/science.abc6500

The PDF file includes:

Other Supplementary Material for this manuscript includes the following:

Materials and Methods

Plasmids

Construct Name	Internal reference	Figure panels
SP64-BCAS2-twinstrep	EZ89	Fig 2A
SP64-MYL6-twinstrep	EZ90	Fig 2A
SP64-CCT3-twinstrep	EZ91	Fig 2A
SP64-PSMC1-twinstrep	EZ136	Fig S10A
SP64-PSMC2-twinstrep	EZ137	Fig 4A, S10A
SP64-PSMC3-twinstrep	EZ138	Fig S10A
SP64-PSMC4-twinstrep	EZ139	Fig 4A, S10A, S11
SP64-PSMC5-twinstrep	EZ92	Fig 2A, 2B, 2C, 3A, 3B, 4A, 5A, S4A, S10A, S10B, S15A
SP64-PSMC6-twinstrep	EZ140	Fig S10A, S11
SP64-PSMC5ΔC-twinstrep	EZ132	Fig 3A, 3B, S10B
SP64-PSMC5-3xFLAG	EZ100	Fig 4A, S4B, S11
SP64-PSMC5ΔC-3xFLAG	EZ148	Fig 4A
SP64 Sec61βΔTMD	2942	Fig 4A
PURE-PSMC5	EZ120	Fig 2D, 3D, 3E, 5B, S5A, S15B
GFP-P2A-mCherry	KY28	Fig S8A
GFP-PSMC5-P2A-mCherry	EZ103	Fig 2F, 3F, S8A, S8B, S13B
GFP-PSMC5ΔC-P2A-mCherry	EZ150	Fig 3C
GFP-PSMC1-P2A-mCherry	EZ141	Fig S9B
GFP-PSMC2-P2A-mCherry	EZ142	Fig 2F
GFP-PSMC3-P2A-mCherry	EZ143	Fig S9B
GFP-PSMC4-P2A-mCherry	EZ144	Fig 4B, S9B
GFP-PSMC6-P2A-mCherry	EZ145	Fig S9B
GFP-BCAS2-P2A-mCherry	EZ122	Fig 2F
GFP-MYL6-P2A-mCherry	EZ123	Fig S9A
GFP-CCT3-P2A-mCherry	EZ121	Fig S9A
GFP-PSMB4-P2A-mCherry	EZ124	Fig S9A
GFP-TSC2-P2A-mCherry	EZ116	Fig S9A
pGEX-3xFLAG-CaM	EZ70	Fig 3E
pcDNA-3xFLAG-HERC1	EZ127	Fig 2D, 3D, 3E, 5A, 5B, S5B, S13B, S14, S15A, S15B, S15C, S15D, S15E
pcDNA-3xFLAG-HERC1(G483E)	EZ180	Fig 5A, 5B, S14, S15A, S15B, S15C, S15D, S15E
pcDNA-3xFLAG-HERC1ΔRLD1	EZ175	Fig 5A, 5B, S13B, S14, S15A, S15B, S15C, S15D, S15E
pcDNA-3xFLAG-HERC1ΔSPRY	EZ176	Fig 5A, 5B, S13B, S14, S15A, S15B
pcDNA-3xFLAG-HERC1ΔWD40	EZ177	Fig S13B, S14, S15A, S15B
pcDNA-3xFLAG-HERC1ΔRLD2	EZ178	Fig S13B, S14, S15A, S15B
pcDNA-3xFLAG-HERC1ΔHECT	EZ179	Fig 5A, 5B, S13B, S14, S15A, S15B

pcDNA-twinstrep-HERC1(3975-C)	EZ114	Fig 2D, S5B
pcDNA-3xFLAG-PAAF1	EZ125	Fig 2D, 3D, 3E, 5B, S5A, S15B
pcDNA-twinstrep-PAAF1	EZ131	Fig S13B
pcDNA-twinstrep-PAAF1 siRNA resistant	EZ172	Fig 3F, 3G
pcDNA-3xFLAG-PSMD10	EZ158	Fig 3D
pcDNA-PSMC5-twinstrep	EZ130	Fig 4B
MXS_CMV::PuroR-bGHpA	Addgene 62439	Fig S12

Constructs for in vitro translation in rabbit reticulocyte lysate (RRL) were cloned from HEK293T cDNA into a pSP64-based vector with C-terminal twin-strep tag (TST) or 3x-FLAG tags. C-terminally truncated PSMC5 was created by deleting the final 86 codons of the full-length construct. The PSMC5 construct for in vitro translation in the PURE system was similar to that in pSP64, but in the T7-based PURExpress plasmid from New England Biolabs. The dual colour fluorescent reporter constructs were based on a construct described previously (24), with coding sequences inserted between GFP and the viral P2A sequence, which was followed by RFP. Constructs for mammalian expression were cloned into pcDNA3.1 (Thermo Fisher), with N-terminal 3xFLAG tag or TST for PAAF1 and HERC1, and C-terminal TST for PSMC5. Full length HERC1 with an N-terminal 3xFLAG tag and TEV cleavage site was created by PCR amplification of 6 fragments from HEK293T cDNA and previously made plasmids, and ligation of fragments and pcDNA vector via NEBuilder HiFi DNA Assembly (New England Biolabs). Mouse calmodulin with an N-terminal 3xFLAG tag was cloned downstream of the 3C protease site in the pGEX vector (GE Healthcare).

siRNAs and sgRNAs

Pre-designed Silencer Select siRNAs were obtained from Thermo Fisher:: s17067, s17066, s17065 for HERC1 knockdowns, and s37098 for PAAF1 knockdown. To make HERC1 knockout MCF7 cells, the following guide RNAs were cloned into px459: GAACCAACCAGAACATCGGA for knockout clone 1 and TTTGATGTGGCGCGATTCCG for knockout clone 2. Guide RNAs for CRISPRa experiments were designed with Broad GPP designer and cloned into the sgRNA(MS2) cloning backbone, a gift from Feng Zhang (Addgene plasmid # 61424).

Reagent	**Source**	**Catalog No.**	**Application**
Silencer Select Negative Control siRNA #1	Thermo Fisher	4390843	Control knockdown
Silencer Select Pre-designed siRNA against HERC1 #1	Thermo Fisher	siRNA ID #s17065	HERC1 knockdown
Silencer Select Pre-designed siRNA against HERC1 #2	Thermo Fisher	siRNA ID #s17066	HERC1 knockdown
Silencer Select Pre-designed siRNA against HERC1 #3	Thermo Fisher	siRNA ID #s17067	HERC1 knockdown
Silencer Select Pre-designed siRNA against PAAF1	Thermo Fisher	siRNA ID #s37098	PAAF1 knockdown

Guide RNA targeting HERC1 5'-GAACCAACCAGAACATCGGA-3'	This study	n/a	HERC1 knockout clone 1
Guide RNA targeting HERC1 5'- TTTGATGTGGCGCGATTCCG-3'	This study	n/a	HERC1 knockout clone 2
Nontargeting guide RNA 5'-CTGAAAAAGGAAGGAGTTGA-3'	Konermann et al. (*31*)	n/a	CRISPRa control
Guide RNA targeting upstream of HERC1 5'- gCCGCCCAACAGGCCCAGCGC -3'	This study	n/a	CRISPRa HERC1 activation
Nontargeting guide RNA 5'-GCACTACCAGAGCTAACTCA-3'	OriGene	n/a	CRISPRa control
Guide RNA targeting upstream of HERC1 5'-GAGGTGAAAGGGGAACCGAG-3'	This study	n/a	CRISPRa HERC1 activation

Antibodies

Antibody	Source	Catalog No.	RRID	Dilution for blotting	Dilution for IP
Rb anti-HERC1	Bethyl	A301-904A	AB_1524073	1:2000	-
Rb anti-PAAF1	Abcam	ab103566	AB_10711960	1:1000	-
Rb anti-PAAF1	Novus	NBP1-82310	AB_11027143	1:2000	-
Rb anti-strep tag	Abcam	ab76949	AB_1524455	1:5000	-
Ms anti-FLAG-HRP	Sigma-Aldrich	A8592	AB_439702	1:5000-1:10000	-
Rb anti-PSMC5	Abcam	ab178681	n/a	1:2500	-
Rb anti-PSMC5	Bethyl	A300-791A	AB_577239	-	1:100
Rb anti-PSMC4	Bethyl	A303-849A	AB_2620200	-	1:200
Ms anti-TUBB	Sigma-Aldrich	T7816	AB_261770	-	1:300

Recombinant proteins

Full length HERC1, the various HERC1 mutants, PAAF1, and PSMD10 were purified from Expi-293 cells via N-terminal 3xFLAG tags. Cells were transfected at a density of 2-3 x 10^6 cells/ml with 1µg DNA and 3µl polyethylenimine (PEI) per ml of culture. 24-72 hours after transfection, cells were lysed by passing through a 23G needle or douncing in lysis buffer [50 mM HEPES pH 7.4, 100 mM KAc, 5 mM $MgAc_2$, 0.01% digitonin, 1 mM DTT, and 1x protease inhibitor cocktail (Roche)]. Lysates were centrifuged at 16000 rpm in a JA 25.50 rotor (Beckman

Coulter) or 15000 rpm in a tabletop centrifuge (Eppendorf), at 4°C for 15-20 minutes and the supernatant was passed over a column of packed anti-FLAG-M2 agarose (Sigma-Aldrich). Columns were washed with at least 35 column volumes each of lysis buffer, high salt buffer (50 mM HEPES pH 7.4, 400 mM KAc, 5 mM $MgAc_2$, 0.01% digitonin, 1 mM DTT) and physiological salt buffer (PSB: 50 mM HEPES, 100 mM KAc, 5 mM $MgAc_2$). Proteins were eluted with 0.2 mg/ml 3xFLAG peptide (Sigma-Aldrich) in PSB, with two to three sequential elutions incubated for 20 minutes each at room temperature. PAAF1 was concentrated in an Amicon Ultra 0.5ml 30K centrifugal filter (Merck Millipore) by centrifugation for 8 minutes at 14000 x g, and PSMD10 was concentrated in an Amicon Ultra 0.5ml 3K centrifugal filter (Merck Millipore) by centrifugation for 11 minutes at 21000 x g.

The C-terminal fragment of HERC1 was purified from HEK293T cells via an N-terminal TST. Cells were transfected with 15µg DNA and 45µl TransIT-293 transfection reagent (Mirus) per 15cm dish. 48 hours post-transfection, cells were lysed in lysis buffer (50 mM HEPES, 125 mM KAc, 2 mM $MgAc_2$ + 0.01% digitonin + protease inhibitor cocktail) by passing through a 23G needle. Following centrifugation in a tabletop centrifuge at 15000 rpm for 15 minutes at 4°C, the supernatant was incubated with streptacin sepharose (GE Life Sciences) for 1 hour at 4°C with end-over-end mixing. Beads were washed three times in lysis buffer, three times in lysis buffer without digitonin or protease inhibitors, and eluted with 50mM biotin in lysis buffer without digitonin or protease inhibitors for 20 minutes on ice.

GST-3xFLAG-Calmodulin was expressed in the BL21(DE3)pLysS strain of E. coli and purified via the GST tag. Bacteria from 2 L culture were lysed by sonication in 50 mM HEPES-KOH pH 7.5, 500 mM NaCl, 1mM DTT, PMSF, Benzamidine, protease inhibitor cocktail, and DNase. Lysates were clarified by centrifugation at 18000 rpm in a JA 25.50 rotor (Beckman Coulter) at 4°C for 30 minutes, and the supernatant was passed over a column of packed glutathione sepharose 4B (GE Life Sciences). Columns were washed with 30 column volumes of lysis buffer and the bound protein eluted with 10mM reduced glutathione in 50 mM HEPES-KOH pH 7.5 with 500 mM NaCl. The GST tag was removed by overnight incubation at 4°C with 3C protease, and dialysed into 50 mM HEPES with 150 mM NaCl to remove free glutathione. The sample was subsequently passed over a second glutathione sepharose column to remove cleaved GST, and concentrated in an Amicon Ultra-4 10K centrifugal filter (Merck Millipore). Glycerol was added to all purified proteins to 10% final concentration, and proteins were snap frozen in liquid nitrogen.

Mammalian in vitro translation

In vitro transcription was performed as previously described (*48*): PCR products served as the template, and SP6-directed transcription reactions were incubated for 1 hour at 37°C. The transcription reaction was directly used for translation without further purification and constituted 1/20th the total translation reaction volume. Translations in RRL were performed as described previously (*24, 48*). In brief, crude reticulocyte lysate obtained from Green Hectares was pre-treated with micrococcal nuclease to digest endogenous mRNAs, then supplemented with total liver tRNA, free amino acids (except methionine), ATP, GTP, creatine phosphate, creatine kinase, glutathione, spermidine, and HEPES pH 7.4, KAc, and $MgAc_2$. Translation was initiated by addition of transcript and ^{35}S-methionine (500 µCi/ml) where needed to label nascent proteins. Translation reactions were incubated at 32°C for 30-60 minutes. Immediately after

translation, the samples were placed on ice, and further manipulations were performed at 0-4°C unless otherwise indicated. Analytical reactions were performed on a scale of 10-30µl, while translations used for identification of binding partners were 1ml reactions.

PURE in vitro translation

Translations in the PURE system (Protein synthesis Using Recombinant Elements) were performed as described previously, using reagents prepared in-house (*49, 50*). Translation reactions were assembled with PSMC5 plasmid DNA at 10 ng/µl, and ^{35}S-methionine at 1 µCi/µl. In Fig. 2D and fig. S5, recombinant PAAF1 was included at 1 µM where indicated. To prepare complexes for the experiment in Fig. 3D, 5B, and fig. S15B, recombinant PAAF1 was included at 6 µM, and recombinant CaM at 15 µM with 100 nM $CaCl_2$. After translation at 37°C for 60-80 minutes, reactions were diluted in PSB and layered onto a 5-25% sucrose gradient (Fig. 2D, 3D, 5B, fig. S5, and fig. S15B) or 20% sucrose cushion in PSB (Fig. 3E). Preparation of sucrose gradients is described in further detail below. Samples were centrifuged in a TLS-55 rotor (Beckman Coulter) at 55000 rpm at 4°C with slow acceleration and deceleration for 2 hours 25 minutes or 60 minutes for the gradient and cushion, respectively. Following centrifugation, 20 µl fractions were taken and analysed by autoradiography. Fractions containing soluble PSMC5 were combined and used in further assays.

Ubiquitination reactions

Radiolabelled substrates for ubiquitination, either on beads (fig. S4A) or in solution (Fig. 2D, 3D, 3E, 5B, fig. S15B), were mixed with 1 mM ATP, 10 mM creatine phosphate, 40 µg/ml creatine kinase, 10 µM His-Ubiquitin, 100 nM human GST-UBE1, and 250 nM UBCH5a in PSB. Ubiquitination reagents were obtained from Boston Biochem. Where indicated, recombinant HERC1 was added at 8-30 nM. Reactions were incubated for 30 minutes at 32°C, and stopped by denaturation in 1% SDS and boiling at 95°C. Ubiquitinated products were recovered by His-Ubiquitin pulldown. In brief, samples were diluted 10-fold in pulldown buffer (1x PBS, 250 mM NaCl, 0.5% Triton X-100, 20 mM imidazole) and incubated with Ni-NTA agarose (Qiagen) for 1.5-2.5 hrs at 4°C. Resin was washed 3 times in pulldown buffer, and samples eluted by boiling in sample buffer supplemented with 50 mM EDTA.

Sucrose gradient centrifugation

Analytical scale 0.2 mL gradients were prepared in 7 × 20 mm centrifuge tubes (Beckman Coulter, 343775) by successively layering 40 µL each of 25%, 20%, 15%, 10%, and 5% sucrose (w/v) in PSB. Gradients were then allowed to stand for 30-60 minutes at 4°C. In vitro translation reactions (up to 20 µL) were loaded on top of the gradients, and the samples centrifuged in a TLS-55 rotor at 55000 rpm at 4°C with slow acceleration and deceleration. Spin time was 45 min for Fig. 2C and fig. S15E, and 145 min for fig. S5A. Eleven 20 µL fractions were successively collected from the top and used directly for downstream analysis.

Affinity purification

Affinity purifications under native conditions were performed by diluting in vitro translation reactions in PSB to 1ml total volume. Samples were incubated with 10-15 µl of anti-FLAG-M2 affinity resin (Sigma-Aldrich) for FLAG immunoprecipitations or streptactin sepharose (Iba Life Sciences and GE Life Sciences) for TST pulldowns for 60-90 minutes at 4°C. The resin was then

washed 5 times in PSB, and transferred to a new tube. For FLAG pulldowns, proteins were eluted sequentially with 0.2 mg/ml 3xFLAG peptide (Sigma-Aldrich) in PSB followed by SDS-PAGE sample buffer. For TST pulldowns, proteins were eluted by boiling in SDS-PAGE sample buffer supplemented with 2 mM biotin. Denaturing anti-FLAG affinity purification was performed by diluting in vitro translation reactions in 100 mM Tris pH 8 with 1% SDS, and boiling for 5 minutes at 95°C. Samples were then diluted 10-fold in IP buffer (50 mM HEPES pH 7.5, 150 mM NaCl, 1% Triton X-100), and incubated 90 minutes at 4°C with 10 µl of anti-FLAG-M2 affinity resin. The resin was washed 3 times in IP buffer, and proteins eluted by boiling in 100 mM Tris pH 8 with 1% SDS. Anti-PSMC5 and anti-PSMC4 affinity purifications were performed by lysing cells in 100 mM Tris pH 8 with 1% SDS and boiling. Denatured cell lysates were diluted 10-fold in IP buffer (as above), centrifuged for 10 min at 15000 rpm in a tabletop centrifuge, and incubated with primary antibody for 1 hr at 4°C. Next, 7.5ul of Protein A affinity resin (Repligen) washed in IP buffer was added to the lysates and incubated for a further 2 hrs at 4°C. The resin was washed 3 times in IP buffer, and proteins were eluted by boiling in sample buffer.

Ubiquitinated products were recovered by Ni-NTA affinity purification for His-Ubiquitin. Reactions were first denatured by boiling in 100 mM Tris pH 8 with 1% SDS. Samples were then diluted 10-fold in pulldown buffer (1x PBS, 250 mM NaCl, 0.5% Triton X-100, 20 mM imidazole) and incubated with Ni-NTA agarose (Qiagen) for 1.5-2.5 hrs at 4°C. Resin was washed 3 times in pulldown buffer, and samples eluted by boiling in sample buffer supplemented with 50 mM EDTA.

HERC1 co-immunoprecipitation in cells

HEK293T cells in 6-well plates were co-transfected with 400ng GFP-PSMC5-P2A-RFP, 500ng TST-PAAF1, and 900-1600 ng FLAG-HERC1 DNA, previously optimized to achieve approximately equal HERC1 expression. After 24 hours, cells were lysed on ice in PSB with 0.1% Triton X-100 and 1mM DTT. Insoluble material was removed by ultracentrifugation at 100,000 rpm for 30 min. Supernatants were incubated with magnetic GFP-trap beads (Chromotek) for 90 min at 4°C. Beads were washed 5 times with lysis buffer and eluted in sample buffer. Input and elution samples were subsequently analysed by immunoblotting.

HERC1 co-immunoprecipitation in vitro

Recombinant FLAG-HERC1 was added to RRL at 2nM (approximately 2-fold lower concentration than the endogenous protein). PSMC5-TST was translated for 45 minutes at 32°C, as above, and subsequently diluted to 1ml with PSB. Affinity purification of PSMC5-TST was performed under native conditions as described above and eluted by heating in SDS-PAGE sample buffer. Input and elution samples were subsequently analysed by immunoblotting.

Cell culture

MCF7 cells (AstraZeneca Global Cell Bank ID 76305) and HEK293T cells (RRID:CVCL_0063) were cultured in DMEM supplemented with 10% fetal bovine serum (FBS). MCF10a cells (AstraZeneca Global Cell Bank ID 77369) were cultured in DMEM/Nutrient Mix F12 Ham (Sigma) supplemented with 5% horse serum (Gibco), 1x GlutaMAX (Gibco), 10 ug/ml insulin (Sigma), 0.5 ug/ml hydrocortisone (Sigma), 0.1 ug/ml cholera toxin (Sigma) and 20 ng/ml EGF (Sigma). Expi-293 cells (Gibco, A14527) were grown in Expi293 expression medium (Gibco,

A1435101). MCF7 cells stably expressing CRISPR dCas9-VP64 and MS2-P65-HSF1 were obtained from GeneCopoeia and cultured in DMEM supplemented with 10% FBS, 10 ug/ml insulin, 8 ug/ml blasticidine, and 200 ug/ml hygromycin. CRISPR-Cas9 mediated gene disruption of HERC1 was performed as previously described (*51*). In brief, MCF7 cells were transfected with px459 plasmid (Addgene) encoding Cas9 and gRNA targeted to HERC1. 24-48 hours after transfection, puromycin was added at 2 μg/ml to select for transfected cells. After an additional 24-48 hours, single cells were transferred to 96 well plates using a MoFlo High Speed Cell Sorter (Beckman Coulter) or serial dilution to an average density of 0.5 cells/well, and subsequently expanded. Successful knockout was verified by western blot for HERC1 (Bethyl Laboratories, A301-904A) in both clones, as well as TIDE sequencing for the primary clone used in most experiments. Cells were transfected with siRNA using Lipofectamine RNAiMAX (Thermo Fisher), and with DNA using TransIT-293 (Mirus) for HEK293T cells or FuGENE HD (Promega) for MCF7 cells, all according to the manufacturers' instructions.

Metabolic labelling

For labelling with ^{35}S-methionine or azidohomoalanine (AHA), cells were first washed in PBS and incubated for 20-30 minutes at 37°C in DMEM lacking serum and methionine (Sigma-Aldrich, D0422), supplemented with 200 μM cysteine and Glutamax. ^{35}S-Met was subsequently added at 100 μCi/ml and AHA at 4 mM, unless otherwise indicated, for 30-60 minutes. Cells were then washed in PBS and chased in serum-containing complete medium or harvested, as appropriate. Cells were harvested by scraping into in ice-cold PBS, sedimented by centrifugation, and resuspended in urea buffer (50 mM HEPES, 150 mM NaCl, 8M urea, 1% CHAPS). The lysate was dispersed by passing through a 26G needle and clarified in a microcentrifuge at 15000 rpm for 10 minutes at 4°C. The clarified cell lysates were either processed immediately (see below) or stored at -20°C for later use. In pulse-chase experiments to monitor endogenous PSMC5 degradation, MCF7 cells were labelled with ^{35}S-Met at 100 μCi/ml for 60 minutes, washed in PBS, chased in complete medium, and lysed in a denaturing buffer containing 100 mM Tris, pH8 and 1% SDS. After heating to 95°C for 5 minutes, lysates were diluted 10-fold in IP buffer (50 mM HEPES, 150 mM NaCl, 1% Triton X-100), and centrifuged for 10 min at 15000 rpm to remove insoluble material. Supernatants were incubated with primary antibody at concentrations detailed above for 1 hour at 4°C, and a further 2 hours at 4°C with 7.5 μl protein A resin (Repligen). Beads were washed 3 times in IP buffer and eluted in sample buffer for analysis by SDS-PAGE and autoradiography. Densitometry was performed with Fiji software.

CRISPRa

MCF7 cells stably expressing CRISPR dCas9-VP64 and MS2-P65-HSF1 were transfected with nontargeting sgRNA or sgRNA against HERC1, along with a plasmid carrying a puromycin selection cassette. The day after transfection, cells were incubated with 2 μg/ml puromycin for 48 hours to select for transfected cells. Cells were subsequently seeded in 12 well plates without puromycin. The following day, cells were incubated with 10 μM MG132 or an equivalent volume of DMSO for 90 minutes in full medium, with three technical replicates per condition. For radiolabelling, cells were first washed in PBS and incubated for 30 minutes at 37°C in DMEM lacking methionine (Sigma-Aldrich), but supplemented with MG132 or DMSO, as previously. ^{35}S-Met was then added at 100 μCi/ml for 60 minutes at 37°C. Cells were lysed in a denaturing buffer containing 100 mM Tris, pH8 and 1% SDS, boiled, diluted 10-fold in IP buffer

(50 mM HEPES, 150 mM NaCl, 1% Triton X-100), and centrifuged for 10 min at 15000 rpm to remove insoluble material. Supernatants were incubated with primary antibody at concentrations detailed above for 1 hour at 4°C, and a further 2 hours at 4°C with 7.5 µl protein A resin (Repligen). Beads were washed 3 times in IP buffer and eluted in sample buffer for analysis by SDS-PAGE and autoradiography. Densitometry was performed with Fiji software, normalized to the same background band in all lanes, and graphs were plotted with Graphpad Prism.

Flow cytometry

Cells growing in 6-well plates were transfected with fluorescent reporter constructs using Fugene HD (Promega), according to the manufacturer's instructions. 48 hours after transfection, cells were trypsinized, washed in phosphate-buffered saline (PBS), and resuspended in 10% FBS in PBS with 1 µg/ml DAPI as a viability marker. Cells were subsequently analysed on a Beckton Dickinson LSRII or LSRFortessa flow cytometer, and data was analysed using FlowJo software. At least 1500 transfected cells were analysed, with the majority of experiments containing ~10000 transfected cells. Each experiment is internally controlled and the control cells shown in each graph were grown, collected, and analysed in parallel with the experimental sample. Unless specifically indicated otherwise, numerical values of fluorescence intensity cannot be directly compared across experiments because the absolute number is dependent on the model of flow cytometer, the settings, and calibration. In general, however, we used detector settings such that the control reporter containing untagged GFP and RFP generates equal GFP and RFP fluorescence values that fall on a diagonal line across a wide range of intensities (fig. S8A).

AHA pulse-chase

MCF7 cells at approximately 50% confluence were grown in 15cm dishes. 24 hours after seeding, cells were washed twice in pre-warmed PBS at 37°C and incubated for 30 minutes at 37°C in DMEM lacking serum and methionine (Sigma-Aldrich, D0422). AHA was then added at 4 mM for 1 hour at 37°C. Following the labelling period, cells were washed in PBS and returned to regular growth medium for the chase timepoints, as indicated. Cells were harvested by scraping into PBS and centrifugation at 1000 rpm for 5 minutes. Cell pellets were resuspended in urea lysis buffer (50 mM HEPES, 150 mM NaCl, 8 M urea, 1% CHAPS) and frozen at -20°C for downstream analysis as described below.

Click chemistry

Clarified cell lysates in urea lysis buffer were reduced with 3 mM DTT and alkylated with 16.5 mM iodoacetamide (IAA) for one hour each at room temperature. Aminoguanidine HCl was added to 5 mM final concentration as a dehydroascorbate scavenger. The lysate was then mixed with 100 µl alkyne agarose (Jena Bioscience) and adjusted to 1 mM $CuSO_4$, 1 mM Tris(3-hydroxypropyltriazolylmethyl)amine (THPTA, Sigma-Aldrich), and 2 mM sodium ascorbate. After incubation for 1 hour at room temperature, the resin was washed 5 times each with SDS wash buffer (100mM Tris pH 8, 1% SDS, 250mM NaCl, 5mM EDTA), 8M urea in 100 mM Tris pH 8, and 20% acetonitrile. The washed resin was analysed by either mass spectrometry or scintillation counting [in 3 ml scintillation cocktail (ULTIMA GOLD, Perkin Elmer) measured in a scintillation analyser (PerkinElmer)]. The click reactions for the analytical experiment using biotin-alkyne (fig. S1E) were for 1 hour at 30°C and contained 100 µM biotin-PEG4-alkyne (Sigma-Aldrich), 1 mM Tris[(1-benzyl-1H-1,2,3-triazol-4-yl)methyl]amine (TBTA; Sigma-

Aldrich), and 0.2 mM $CuSO_4$. The reaction was then precipitated with trichloroacetic acid, washed in acetone, and resuspended in SDS-PAGE sample buffer. Samples were analysed by SDS-PAGE, blotting to nitrocellulose, and detection using horseradish peroxidase (HRP) conjugated to streptavidin.

Mass spectrometry

Protein samples on beads were reduced with 10 mM DTT at 56°C for 30 minutes and alkylated with 15 mM IAA for 30 minutes in the dark at 22°C. The alkylation reaction was quenched by the addition of DTT and the samples were digested on beads with trypsin (Promega) overnight at 37°C. After this, each supernatant was transferred to a fresh Eppendorf tube, the beads were extracted once with 50% acetonitrile/ 0.1% TFA and combined with the corresponding supernatant. The peptide mixtures were then partially dried in a SpeedVac and desalted using home-made C18 (3M Empore) stage tip that contained 2 µl poros R3 (Applied Biosystems) resin. Bound peptides were eluted sequentially with 30%, 50% and 80% acetonitrile in 0.1%TFA and lyophilized.

Where TMT labeling was required, dried peptide mixtures from each condition were re-suspended in 20 µl of 7% MeCN, 200 mM triethyl ammonium bicarbonate. 0.8 mg of TMT reagents (Thermo Fisher Scientific) were reconstituted in 41 µl anhydrous MeCN. 10 µl of different TMT labels was added to each peptide mixture and incubated for 1 hr at room temperature. The labeling reactions were terminated by incubation with 2.5 µl 5% hydroxylamine for 15 minutes. The labeled samples were pooled, transferred to a SpeedVac to remove acetonitrile, desalted and then fractionated with home-made C18 stage tip using 10 mM ammonium bicarbonate and acetonitrile gradients. Eluted fractions were acidified, partially dried down in a SpeedVac and subsequently used for for LC-MS/MS.

Liquid chromatography was performed on a fully automated Ultimate 3000 RSLC nano System (Thermo Fisher Scientific) fitted with a 100 µm x 2 cm PepMap100 C18 nano trap column and a 75 µm × 25 cm reverse phase C18 nano column (Aclaim PepMap, Thermo Fisher Scientific). Samples were separated using a binary gradient consisting of buffer A (2% MeCN, 0.1% formic acid) and buffer B (80% MeCN, 0.1% formic acid). Peptides were eluted at 300 nL/minute with an acetonitrile gradient. The HPLC system was coupled to a Q Exactive Plus hybrid quardrupole-Orbitrap mass spectrometer (Thermo Fisher Scientific) equipped with a nanospray ion source.

For protein identification by mass spectrometry, on bead trypsin digestion and LC-MS/MS was performed as above. Data were searched against the mammalian UniProt database (2016) using Mascot (v 2.4, Matrix Science), with a precursor tolerance of 10 ppm and two trypsin missed cleavages. Carbamidomethylation of cysteines was set as fixed modification, while methionine oxidation and N-terminal protein acetylation as variable modifications. MS/MS data were validated using the Scaffold program (Proteome Software Inc).

For TMT experiments, the acquired raw files from LC-MS/MS were processed using MaxQuant (*52*) with the integrated Andromeda search engine (v.1.5.5.1 or v.1.6.6.0 [AHA]). MS/MS spectra were quantified with reporter ion MS2 from TMT 10-plex experiments and searched against Homo sapiens reviewed, UniProt Fasta database (March19). Carbamidomethylation of cysteines was set as fixed modification, while methionine oxidation, N-terminal protein acetylation, (also Met replaced by AHA and Met replaced by AHA reduced

for AHA experiment) were set as variable modifications. Precursor tolerance of 10 ppm and two trypsin missed cleavages were allowed. Protein quantification requirements were set at 1 unique and razor peptide. In the identification tap, second peptides and match between runs were not selected. Other parameters in MaxQuant were set to default values.

Following data acquisition and processing, tandem mass tag (TMT) intensity for each individual protein was normalized by the total intensity across all proteins at that time point. This normalization is justified because ^{35}S-methionine pulse-chase experiments verified that total protein degradation over 8 hours is minimal. Proteins were assigned an abundance ranking based on the intensity at the 0 hour time-point to cull the dataset to the top 20% most abundant proteins. After normalization and culling of the complete dataset, the relative proportion of each protein's total signal was calculated for each time point (with the sum necessarily adding up to 1) and used to generate the heatmaps displayed in the figures. The heatmaps depict the average of two biological replicates. To produce the graphs illustrating protein degradation (Fig. 1C and fig. S2B), protein levels at each time point were plotted relative to the amount at 0 hours. Unless stated otherwise, the graphs display the average of two biological replicates. The y-axis is displayed as a log scale so that exponential decrease in a protein is seen as linear on the graph, highlighting non-linear decay as indicative of non-exponential decay.

RNA-seq comparative analysis

RNA-seq gene expression data for 1379 cancer cell lines was obtained from Depmap, version 21Q2 (*53*). The numerical values in this dataset are expressed as transcript per million (TPM), normalized and quantified using RSEM (RNA-Seq by Expectation Maximization), and $\log_2$ transformed using a pseudo-count of 1. Thus, the values were used directly without further manipulations. The "normal" expression level for each mRNA was taken to be the average of the expression levels across all 1379 cancer cell lines. This baseline was subtracted from the expression level of individual mRNAs in individual cell lines as an indicator of increased or decreased level of expression. This difference (of $\log_2$ values) was used for the various plots shown in Fig. 1 and fig. S3.

Replication, reproducibility, and statistical analysis

The TMT mass spectrometry data in Fig. 1 represents the average of two independent biological replicate experiments, with the individual data from each experiment shown in table S1. The TMT mass spectrometry experiment in Fig. 2E was independently replicated, and both replicates are shown in the plot, and in table S6. The TMT mass spectrometry experiment in fig. S7 shows the data from three independent biological replicates, with the full dataset in table S7. The plots in fig. S6B, S12D, and S12E show three technical replicates in which three dishes of cells were analyzed for each condition within the shown experiment. Each experiment was repeated independently on another day with similar results. Biochemical and flow cytometry experiments were reproduced at least once with similar results to the examples shown in the paper. Statistical comparisons, where shown in the figures, always employed a two-tailed Student's t test. The resulting p values are indicated in the figure. Error bars are defined in the legends to the figure panels that contain them.

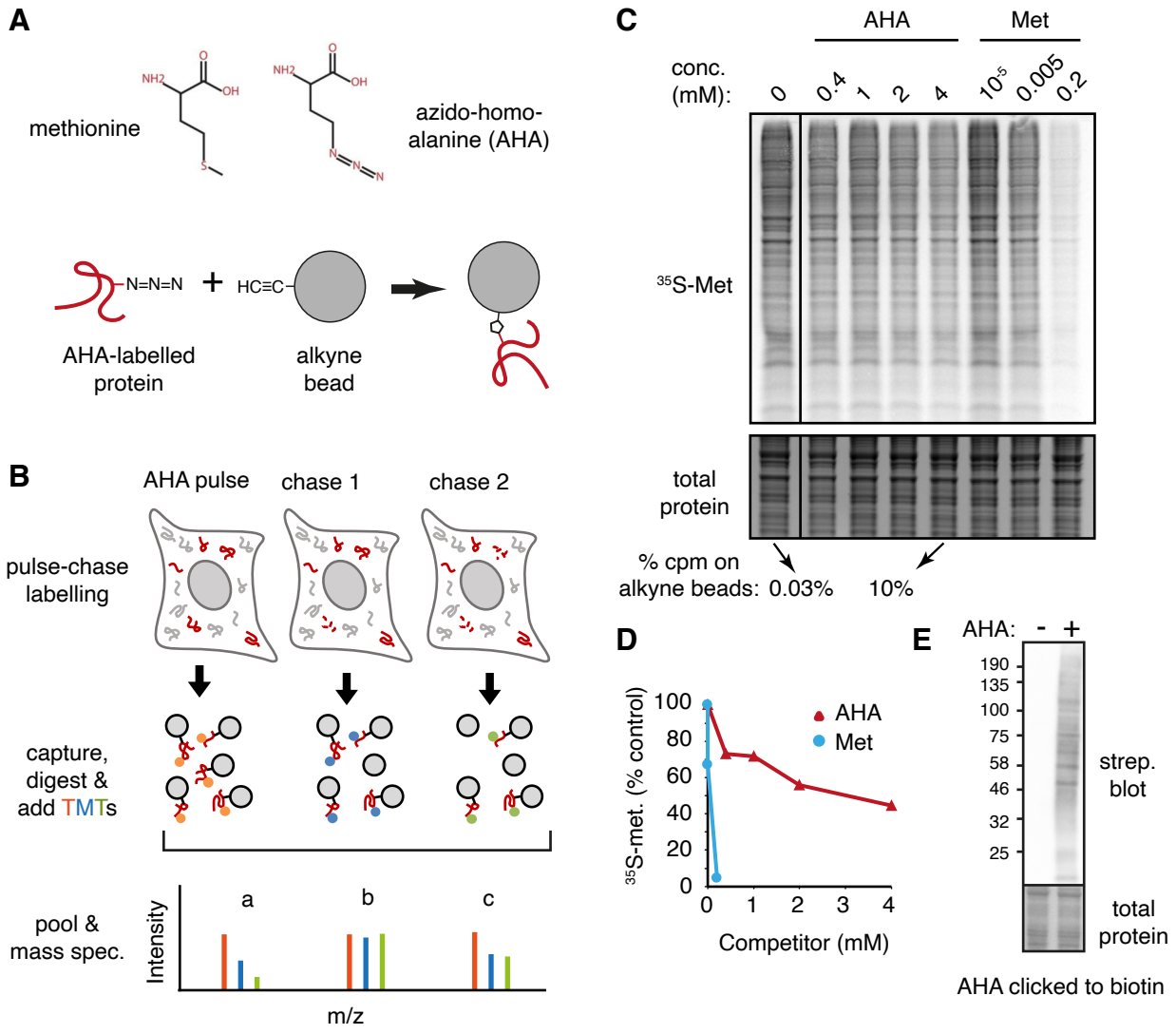

Fig. S1. Characterization of AHA labelling and click chemistry. (**A**) Diagrams illustrating the similarity of azidohomoalanine (AHA) and methionine, and how AHA-containing proteins are captured by beads containing immobilized alkyne using copper-catalyzed cycloaddition (or 'click' chemistry). (**B**) Principles behind pulse-chase mass spectrometry using AHA. The AHA-containing proteins from cells are captured using immobilized alkyne, digested on the beads with trypsin, labeled with tandem mass tags (TMTs), and analyzed as a pooled sample by mass spectrometry. Schematic of the mass spectra illustrates how the fate of three different proteins (a, b, and c) over time can be inferred from the relative amounts of TMT-labelled peptides from those proteins. Orange, blue and green peaks represent the same peptide from the three samples (pulse and two chase points) that are slightly mass-shifted due to different covalently attached mass tags. (**C**) HEK293T cells were pre-incubated for 30 min with methionine- and serum-free media. Then, ^{35}S-methionine was added directly to the media together with the indicated concentrations of either AHA or unlabeled methionine (Met). Cells were harvested after 1 hour of labelling. Autoradiographs of cell lysates (top panel) and a portion of the coomassie stained gel are shown. Aliquots of the indicated cell lysates were 'clicked' to alkyne beads followed by stringent washing. The percent of starting counts per minute (cpm) recovered on the beads (determined by scintillation counting) is indicated. The enrichment above background is ~376-fold. (**D**) Quantified ^{35}S-methionine signal (normalised for total protein) is plotted from the experiment in panel C. 4mM AHA, which results in ~50% competition, was used in subsequent experiments. (**E**) Cell lysates from similarly labelled cells as in panel C without or with 4 mM AHA were 'clicked' to biotin-alkyne and the proteins were analyzed by SDS-PAGE and blotting for biotinylated protein. Note the highly specific biotinylation of proteins only in the lysates from AHA-labeled cells.

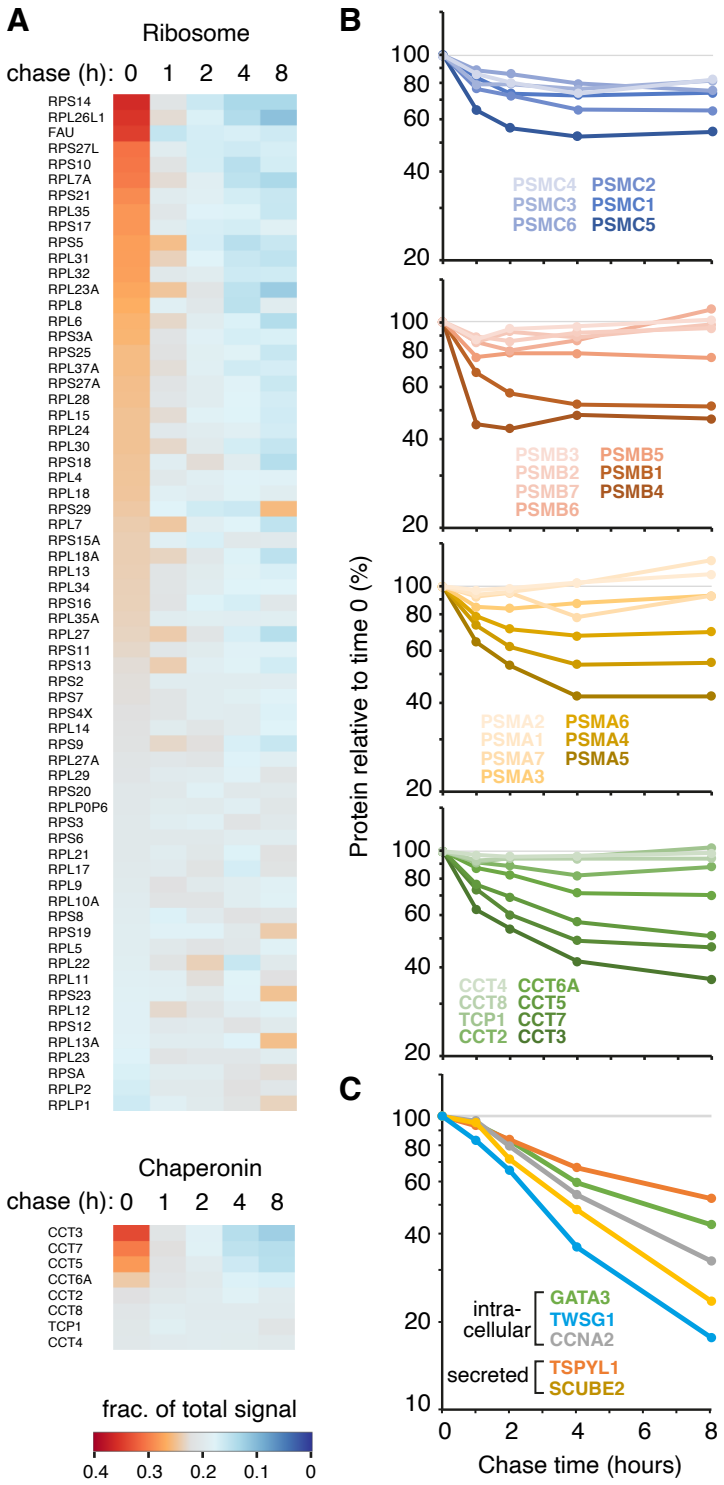

Fig. S2. Individual subunits of multimeric complexes are partially unstable after synthesis. (**A**) Data from the pulse-chase mass spectrometry experiment shown in Fig. 1B are displayed for the ribosome and cytosolic chaperonin. As in Fig. 1B, the heat map for any individual protein represents the proportion of total signal for that protein present at each time point (and hence, the sum across the pulse-chase for each protein is by definition 1.0). For example, a completely stable protein would have a signal of 0.2 at each of the five time points, while a protein that is degraded over time would have a signal higher than 0.2 (i.e., reddish) at time 0 and a signal less than 0.2 (i.e., blueish) at 8 hours. Note that a proportion of some subunits is rapidly degraded within one to two hours after synthesis, with the remainder being comparatively stable thereafter. This is indicative of non-exponential decay caused by a mixture of a rapidly degraded population and a relatively stable population. RPS27, PSMC5, and PSMB4 are particularly clear examples of this behavior. By contrast, other subunits of the same complexes remain stable throughout the duration of the experiment, indicating that the complexes as a whole are not degraded. Examples include RPL23, PSMB3, CCT4, or PSMD2. (**B**) Plots of various proteins over time illustrating the non-exponential decay of some, but not all subunits within a complex or sub-complex (top four graphs). On these plots, in which the y-axis is a log scale, exponential decay would be a straight line (see Fig. 1C). The subunits within each plot are colored such that those with a higher unstable fraction are darker shades. (**C**) The bottom graph shows examples of exponential degradation (GATA3, TWSG1, and CCNA2) and exponential loss due to secretion (TSPYL1 and SCUBE2).

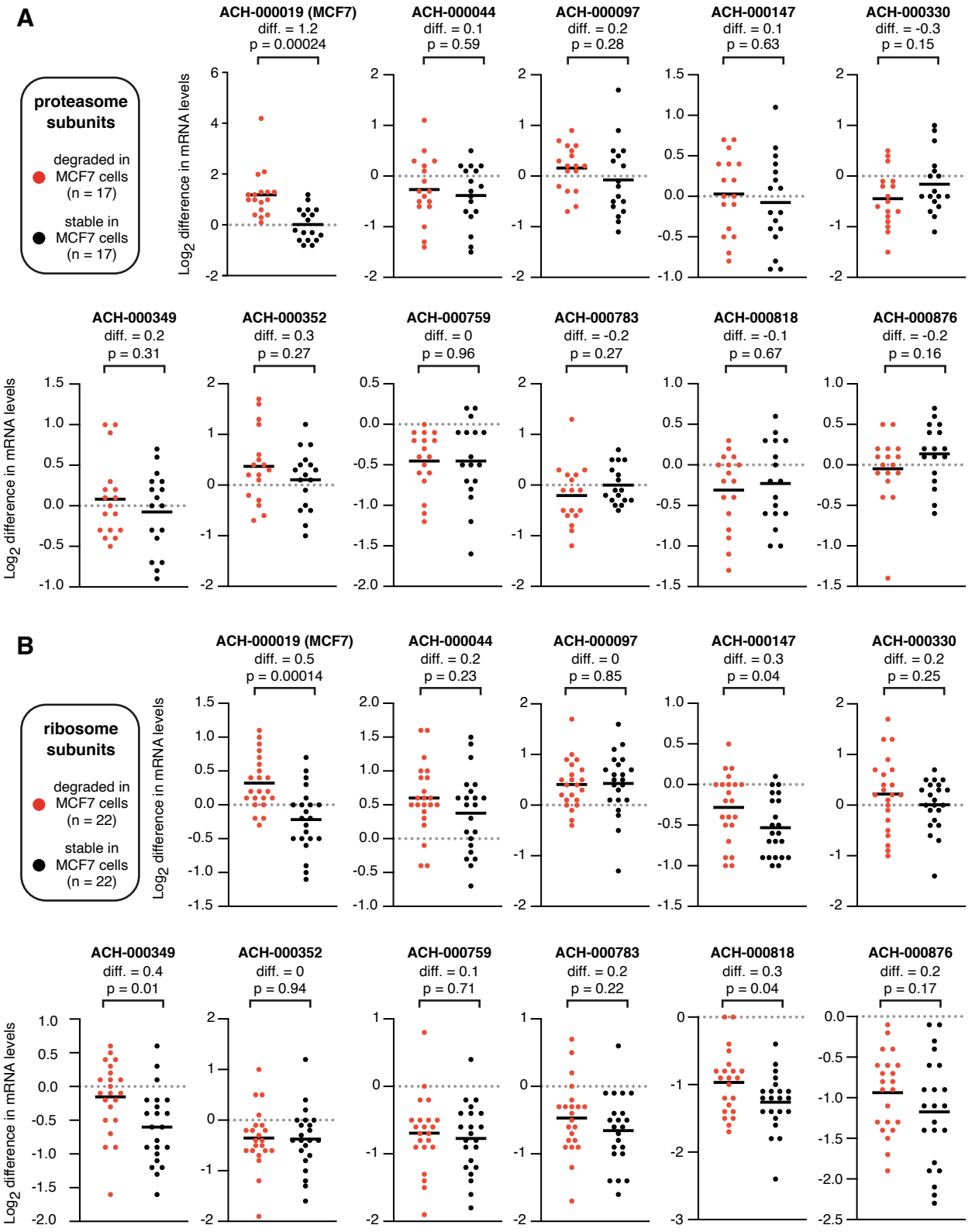

Fig. S3. Relationship between mRNA levels and protein instability. (**A**) Individual mRNA levels in eleven different breast cancer cell lines (identified by their Depmap ID numbers) for proteasome subunits that are either degraded (red dots) or relatively stable (black dots) in MCF7 cells (see Fig. 1B). Each mRNA level is expressed as the $\log_2$ difference from that mRNA's average level across all 1379 cell lines in the DepMap database. Thus, the dotted grey line at zero is by definition the average mRNA level across all 1379 cell lines. The plot for MCF7 cells is reproduced from Fig. 1F for comparison. The $\log_2$ difference between the mean of the red points and black points is indicated, as well as the p value for a Student's two-tailed t-test comparing these two sets of data. The difference is largest in MCF7 cells, which also shows the greatest statistical significance. (**B**) Plot as in panel A but for ribosomal subunits (see fig. S2A). The degraded and stable subunits were defined as the top and bottom third of the ranked list shown in fig. S2A. Note that the difference is largest in MCF7 cells, which also shows the greatest statistical significance.

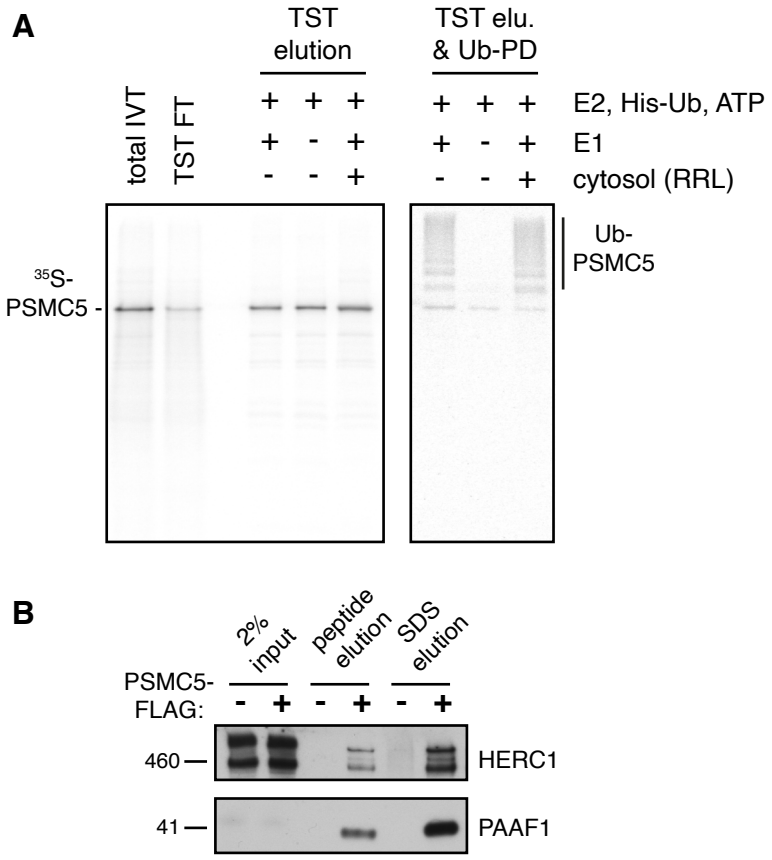

Fig. S4. The ubiquitin ligase HERC1 associates with nascent PSMC5. (**A**) ^{35}S-methionine labelled twin-Strep tagged (TST) PSMC5 was translated in RRL and affinity purified under native conditions using the C-terminal TST. The TST elution fraction was divided into three equal aliquots and incubated with E1, E2 (UBCH5), His-Ub, ATP, and RRL (cytosol) as indicated. A small aliquot of these three reactions was analyzed directly (TST elution) while the remainder was denatured and subjected to ubiquitin pulldown (Ub-PD) using Ni-NTA. ^{35}S-labeled PSMC5 was visualized by autoradiography. All samples were analyzed on the same gel, but the left panel is from a shorter exposure of the autoradiograph than the right panel. (**B**) IVT reactions in RRL lacking or containing mRNA encoding C-terminal FLAG-tagged PSMC5 was subjected to anti-FLAG immunoprecipitation under native conditions. Immunoprecipitates eluted with FLAG peptide or SDS buffer were blotted for HERC1 and PAAF1.

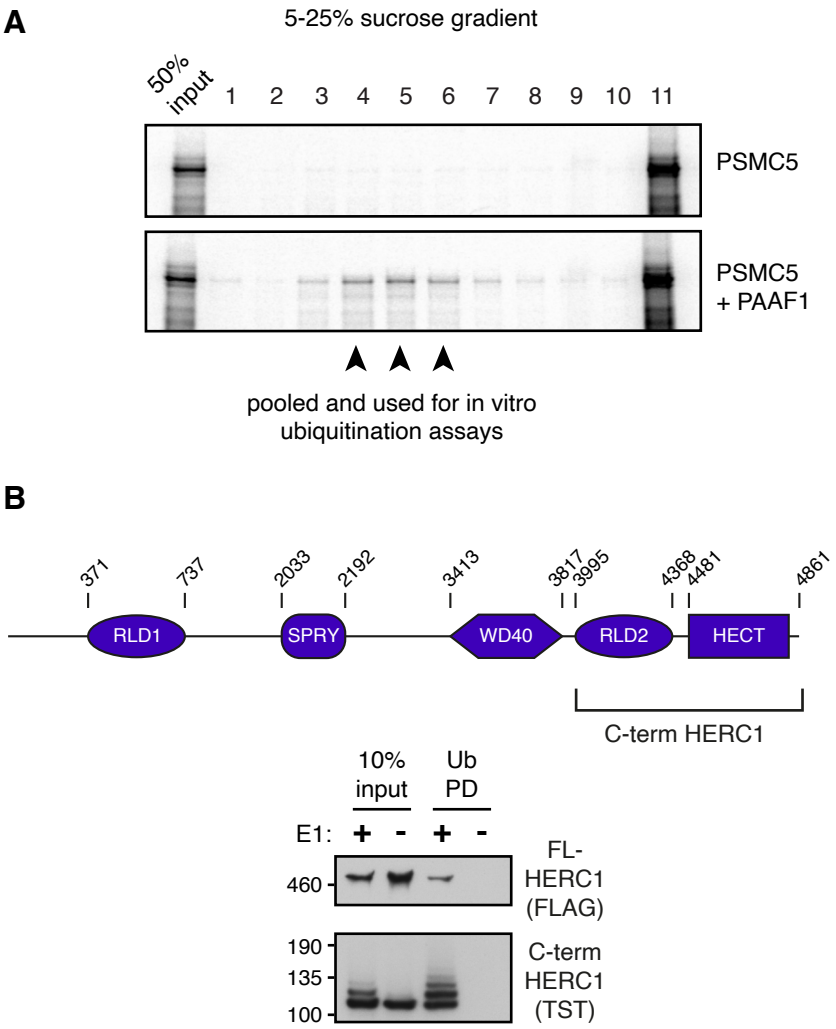

Fig. S5. Preparation of PMSC5-PAAF1 complexes by PURE in vitro translation. (**A**) ^{35}S-methionine labelled PSMC5 was translated in a completely purified translation system (the PURE system; see Methods) consisting of E. coli translation factors. The translation reaction was separated on a 5-25% sucrose gradient and individual fractions analyzed by SDS-PAGE and autoradiography. PSMC5 translated in this system was entirely insoluble and sedimented to the bottom of the gradient (fraction 11). Inclusion of recombinant PAAF1 in the reaction prevented a portion of nascent PSMC5 from aggregating. This soluble PSMC5-PAAF1 complex migrating in fractions 4-6 (arrowheads) was recovered and used as the substrate for in vitro ubiquitination assays shown in Fig. 2D. The PSMC5-PAAF1 complex migrates larger than a ~80 kD protein complex but smaller than a ~160 kD protein complex, suggesting it consists of a single heterodimer of PSMC5 (~ 46 kD) and PAAF1 (~42 kD). (**B**) Purified full-length HERC1 (FL-HERC1) and a truncation mutant containing only the C-terminal region (C-term HERC1) were tested for auto-ubiquitination by incubation with E1, E2 (UBCH5), His-Ub, and ATP. Control reactions contained all components except E1. Ubiquitinated products were recovered by Ni-NTA pulldown under denaturing conditions, and examined by immunoblot against the affinity tag on HERC1 to assess autoubiquitination. Note that C-term HERC1 is small enough to resolve a ubiquitin ladder, whereas FL-HERC1 is not.

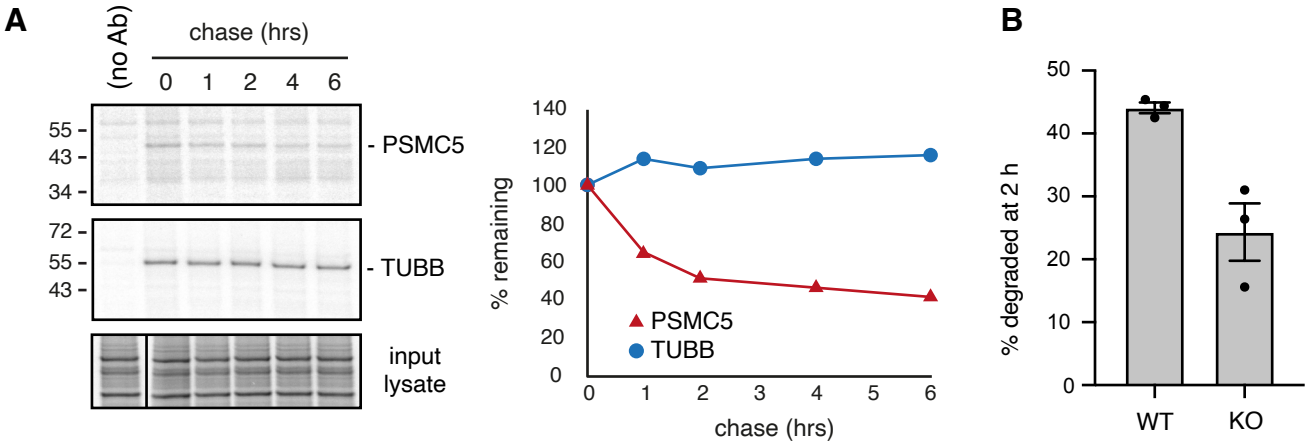

Fig. S6. HERC1 depletion inhibits degradation of endogenous nascent PSMC5. (**A**) MCF7 cells were radiolabelled with ^{35}S-methionine for 1 hour and chased in full medium for the times indicated. Cells were subsequently lysed under denaturing conditions and immunoprecipitated using antibodies against PSMC5 or β-tubulin, a stable housekeeping protein. The first lane is a pulse-labelled sample immunoprecipitated without primary antibody as a specificity control. Immunoprecipitates and input lysates were visualised by autoradiography. Band intensities were quantified by densitometry, normalized according to the intensity of the input lysate, and plotted as a percentage of the pulse time point. (**B**) Wild-type or HERC1 knockout MCF7 cells were radiolabelled for 1 h as in panel A, chased in full medium for 2 hours, and PSMC5 was immunoprecipitated from the pulse and pulse-chase samples under denaturing conditions. The proportion of initial PMSC5 degraded after a 2 h chase was calculated using densitometry. The mean, standard error, and individual data points of 3 replicates are plotted.

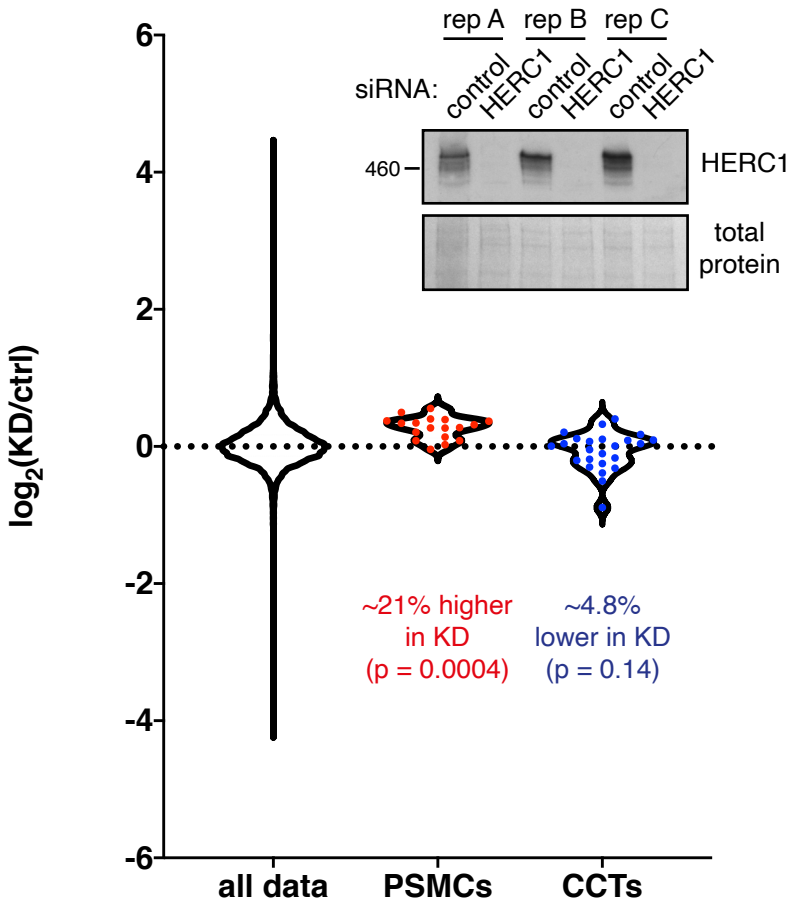

Fig. S7. HERC1 promotes the degradation of 19S ATPases in a non-cancer-derived cell line. MCF10a cells were pretreated with non-targeting control or HERC1-targeting (KD) siRNAs and effective knockdown was verified by immunoblot (see inset). The cells were metabolically labeled for 1 hour with AHA. The labeled proteins were selectively recovered using click chemistry, and analyzed by tandem-mass-tag (TMT) labelled quantitative mass spectrometry. Data from three biological replicates are plotted together as violin plots of the $\log_2$-transformed KD/control ratio. Relative to the full dataset, The 19S ATPases (PSMCs) were significantly stabilized by HERC1 depletion (p=0.0004 by 2-tailed Student's t-test), while subunits of another multimeric complex, the CCT chaperonin, did not differ significantly from the full dataset.

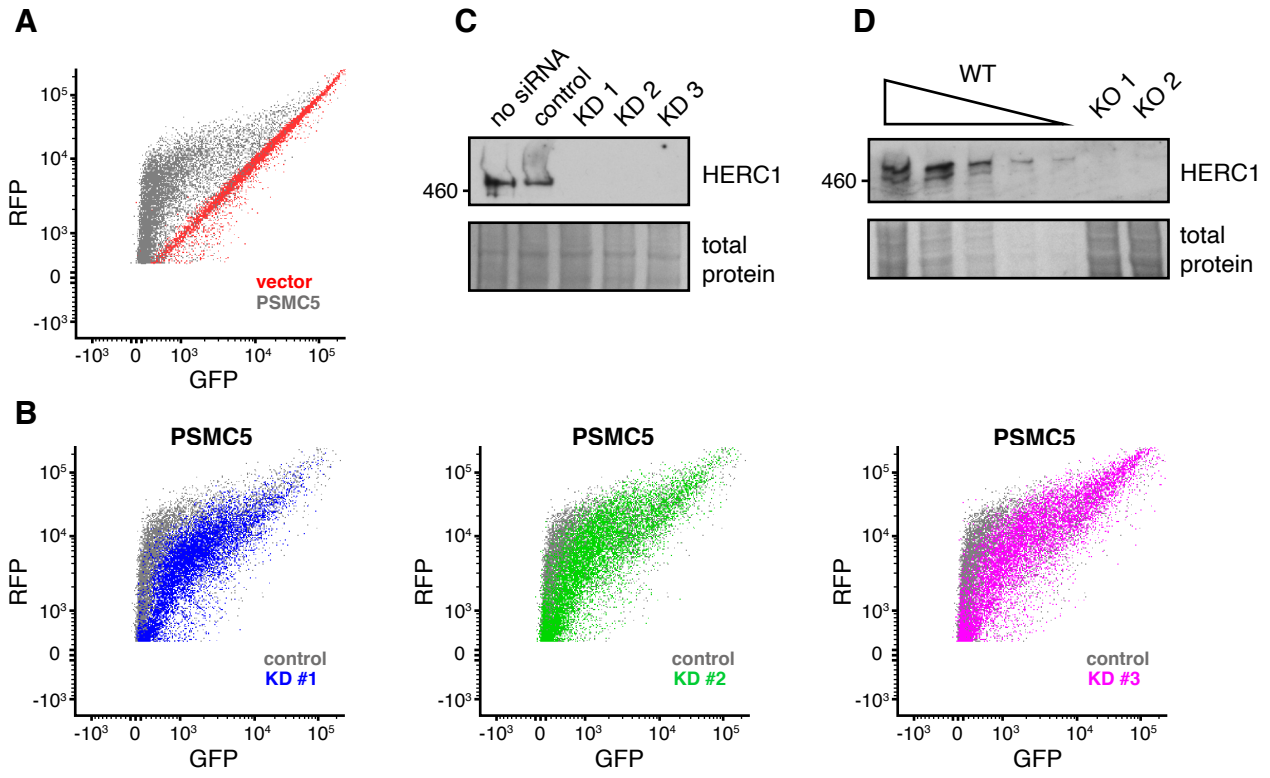

Fig. S8. HERC1 facilitates degradation of a fluorescent PSMC5 reporter. (**A**) GFP-PSMC5 is degraded relative to RFP produced from the same mRNA and separated by a viral P2A sequence. An empty vector containing only GFP and RFP separated by the P2A sequence is shown for comparison. This control reporter shows essentially equal RFP and GFP levels across a very wide range of reporter expression. Hence, the points lie on a diagonal. Note the marked left-shift of the GFP-PSMC5 reporter indicating its reduced levels relative to the internal RFP control. In cells with high reporter expression, the magnitude of the left-shift is reduced, presumably because the degradation pathway for PSMC5 is being saturated. (**B**) HERC1 depletion by three independent siRNAs stabilizes the GFP-PSMC5 reporter. These dot plots correspond to the histogram shown in Fig. 2F. (**C**) Verification of HERC1 knockdown by immunoblot. (**D**) Verification of CRISPR-mediated HERC1 knockout in two independent cell lines generated using two different guide RNAs. HERC1 in WT lysate is detectable in dilutions ranging from 100% to 5%.

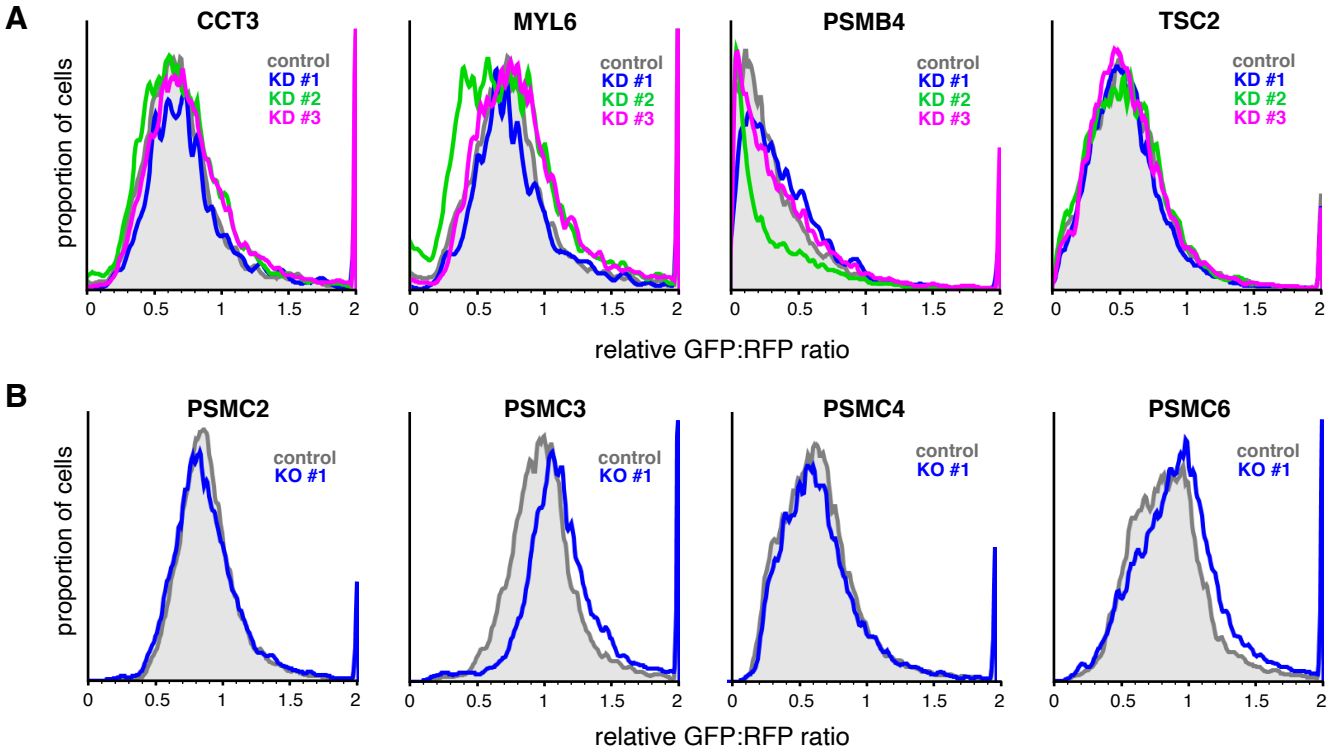

Fig. S9. Analysis of various reporters for HERC1-dependence. (**A**) Flow cytometry analysis of GFP-tagged reporter proteins compared to an internal RFP control in MCF7 cells treated with non-targeting siRNA or siRNA against HERC1, as in Fig. 2F. (**B**) Flow cytometry analysis of GFP-tagged reporters of the 19S ATPase ring subunits in WT and HERC1 knockout MCF7 cells.

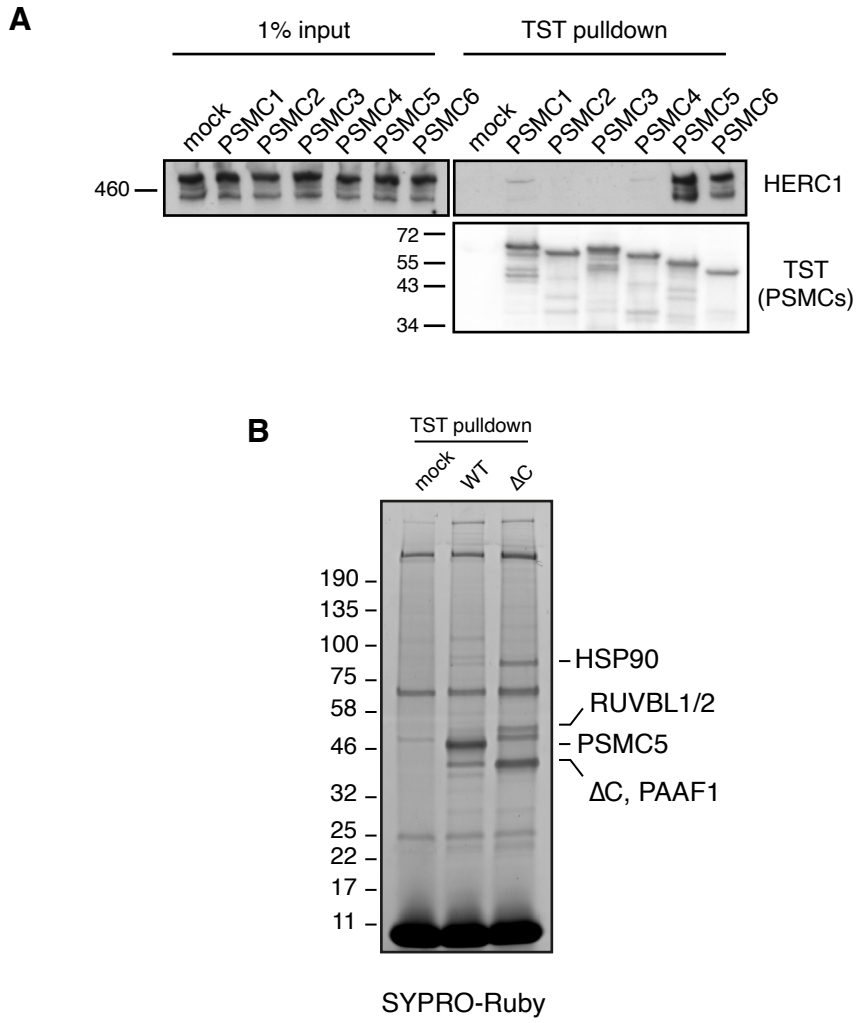

Fig. S10. Analysis of HERC1 interaction with 19S ATPase ring subunits. (**A**) PSMC1 to PSMC6 were translated in RRL and full length products were purified under native conditions using a C-terminal twin-Strep tag (TST). Immunoprecipitates were blotted for HERC1 and TST (to verify equal recovery of the translated PSMCs). As expected, PSMC5 most prominently co-precipitates HERC1, with little or no interaction seen with PSMC1 through PSMC4. PSMC6 does interact with HERC1, even though PSMC6 does not interact directly with PAAF1. The significance of the HERC1-PSMC6 interaction remains to be studied. (**B**) Full length PSMC5 and C-terminally truncated PSMC5 were translated in RRL and purified under native conditions using a C-terminal TST, as in Fig. 3A. Immunoprecipitates were stained with SYPRO-Ruby, and the major bands identified by mass spectrometry are indicated. Note that the loss of HERC1 interaction with PSMC5 upon deletion of its C-terminal domain was verified by immunoblot (see Fig. 3A), but is not evident on this gel due to poor resolution in that size range.

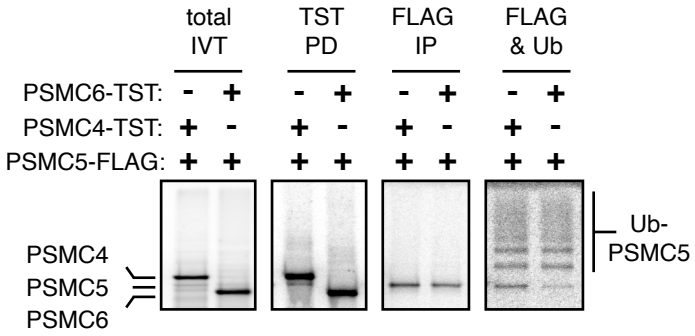

Fig. S11. Assembly with PSMC4 does not protect PSMC5 from ubiquitination. FLAG-tagged PSMC5 was co-translated with excess twin-Strep tagged (TST) PSMC4 or PSMC6 to promote complex formation. The reaction contained both ^{35}S-methionine to visualize the translation products and His-tagged ubiquitin. An aliquot of the total IVT is shown in the first panel. The second panel shows pulldowns using the TST, verifying that PSMC5 is selectively recovered with PSMC4, but not PSMC6. The third panel shows denaturing FLAG IPs verifying that PSMC5 was translated to equal levels in both reactions. The fourth panel shows denaturing FLAG IPs followed by pulldown using His-ubiquitin verifying that ubiquitination of PSMC5 occurs equally well in the sample containing PSMC4 versus the sample containing PSMC6.

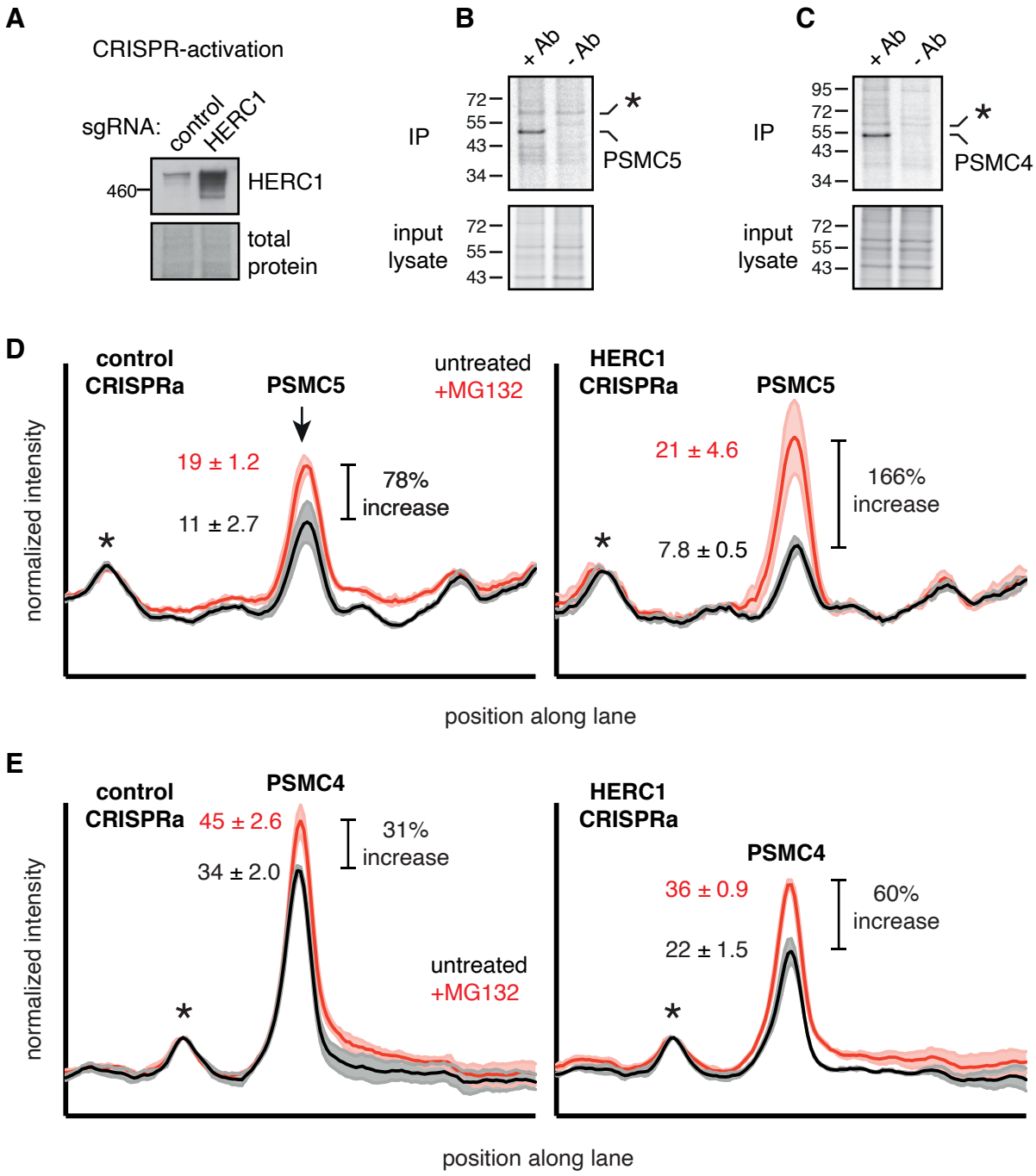

Fig. S12. Increased HERC1 leads to promiscuous degradation of nascent ATPase subunits. (**A**) Validation of CRISPRa. MCF7 cells stably expressing the components for CRISPR-activation (catalytically inactive dCas9 fused to VP64 and the activator helper complex MS2-P65-HSF1) were transfected with sgRNA targeting the HERC1 promoter or a nontargeting control sgRNA. The transfected cells were isolated by antibiotic selection and the levels of HERC1 analyzed by immunoblotting. (**B**, **C**) Validation of PSMC5 and PSMC4 antibodies for immunoprecipitation (IP). MCF7 CRISPRa cells were radiolabelled with ^{35}S-methionine for 1 hour, lysed under denaturing conditions, and subjected to IP using antibodies against PSMC5 or PSMC4, as indicated. Control samples lacked the antibody. The total lysate and IP samples were visualized by SDS-PAGE and autoradiography. The positions of endogenous PSMC5, PSMC4, and a minor non-specific band (*) are indicated. (**D**) MCF7 cells subjected to CRISPRa of HERC1 (or control) were radiolabelled in the absence (black) or presence (red) of the proteasome inhibitor MG132 and immunoprecipitated as in panel C. Each lane of the autoradiograph was quantified by scanning densitometry of the PSMC5 region and normalized to the nearby non-specific band (*). The traces represent the mean ± standard deviation for data from 3 replicate dishes of cells. All of the samples were labelled, IP'd, and analyzed together on the same gel and plotted on the same scale (arbitrary units). The area under the curve for the PMSC5 band was quantified and indicated on the traces. (**E**) Same as panel D but for PSMC4. Note that HERC1 overexpression results in reduced levels of both PSMC5 and PSMC4 relative to cells containing normal HERC1 levels. This reduction is due to promiscuous degradation as evidenced by stabilization in MG132-treated cells. These results for both PSMC5 and PSMC4 were confirmed in independent experiments with a different pair of control and HERC1 sgRNAs.

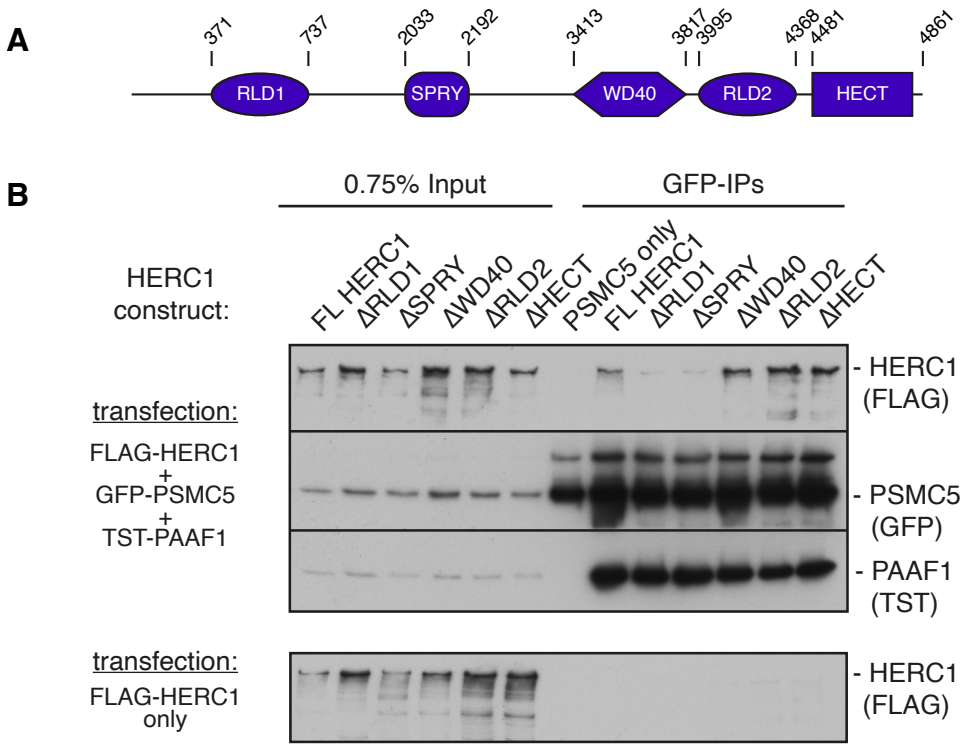

Fig. S13. Characterization of recombinant HERC1 constructs. (**A**) Domain organization of full length human HERC1, with boundaries used for deletion constructs indicated. (**B**) HEK293T cells were transfected with the indicated FLAG-tagged HERC1 constructs with (top panel) or without (bottom panel) GFP-PSMC5 and TST-PAAF1. Native immunoprecipitations (IPs) using GFP-PSMC5 were analyzed with the respective input samples by immunoblotting for the antigens indicated on the right. HERC1 is not precipitated in the absence of GFP-PSMC5 co-expression (bottom panel). Note that the ΔRLD1 construct is recovered inefficiently with GFP-PSMC5 despite being expressed at similar or higher levels than wild type HERC1. The ΔSPRY construct is also recovered at lower levels, but this seems to be due in part to lower overall expression.

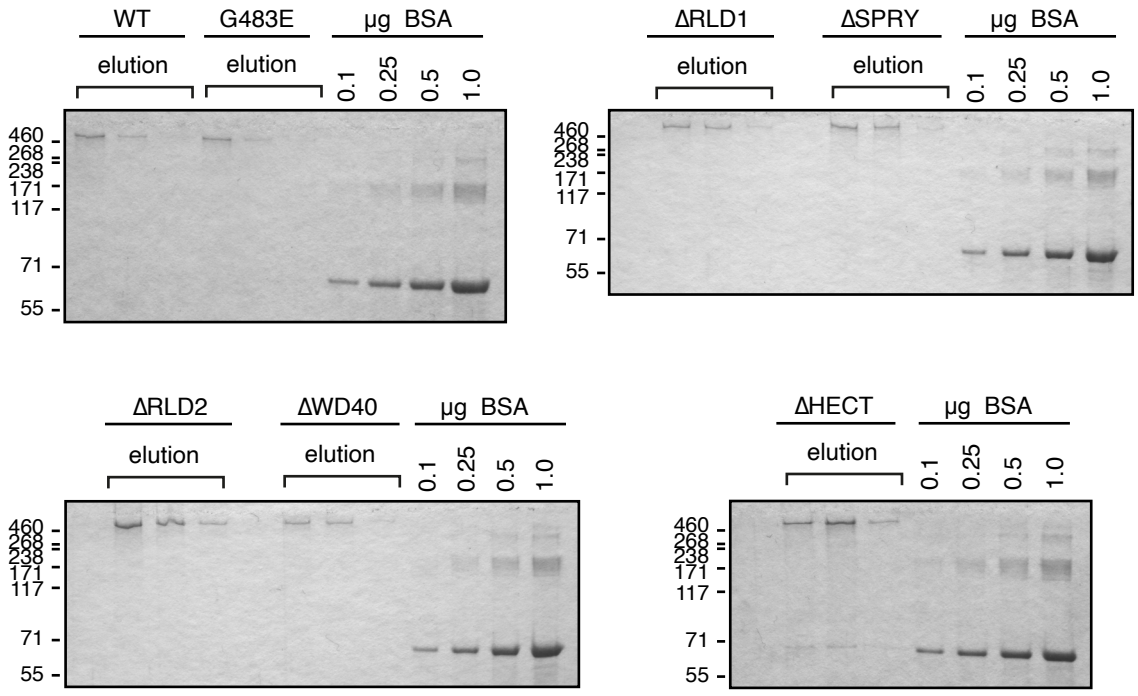

Fig. S14. Purification of recombinant FLAG-HERC1. FLAG-HERC1 constructs were purified from Expi-293 cells using N-terminal 3xFLAG tags, and visualised by Coomassie staining. Eluted proteins were compared to serial dilutions of bovine serum albumin (BSA), demonstrating that the mutant constructs yielded similar amounts of protein as the wild-type construct.

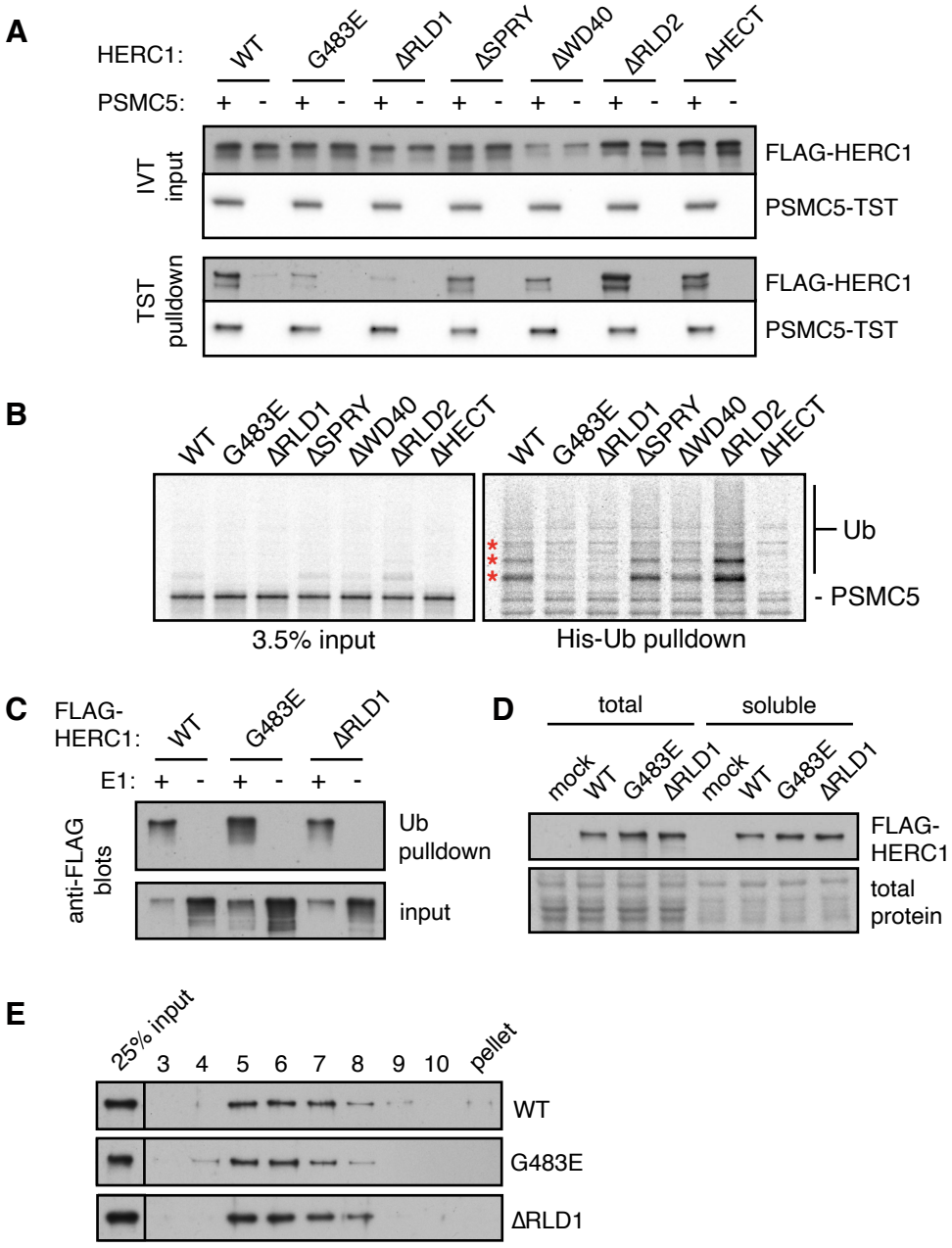

Fig. S15. Characterization of recombinant FLAG-HERC1. (**A**) Recombinant purified FLAG-tagged HERC1 proteins (see fig. S14) were added at 2 nM to RRL in vitro translation reactions with or without mRNA for twin-Strep-tagged (TST) PSMC5. PSMC5-TST was affinity purified under native conditions using Streptactin, and inputs and elutions visualized by immunoblotting. Note that this experiment and that in panel B were performed with a different prep of purified proteins than the experiment in Fig. 5 to verify reproducibility of the results. (**B**) ^{35}S-labeled PSMC5 in complex with PAAF1 was produced by translation in the PURE system (as in fig. S5A). The complex was mixed with E1, E2, His-Ub, ATP, and 8nM wild-type or mutant HERC1. Ubiquitinated products were enriched by Ni-NTA pulldown under denaturing conditions. The input and ubiquitin pulldown samples were visualized by autoradiography. The positions of mono-, di-, and tri-ubiquitinated PSMC5 are indicated with red asterisks (also visible faintly in the input sample). (**C**) Purified FLAG-HERC1 and the indicated mutants were tested for auto-ubiquitination by incubation with E1, E2 (UBCH5), His-Ub, and ATP. Control reactions contained all components except E1. Ubiquitinated products were recovered by Ni-NTA pulldown under denaturing conditions, and examined by immunoblot against the FLAG tag on HERC1 to assess autoubiquitination. Note that a ubiquitin ladder is not visible due to the substrate being ~500 kD. In addition, recognition of the FLAG tag becomes impaired upon ubiquitination, presumably because the lysine residues within the tag are modified. This is why the input signal in samples with active ubiquitination is reduced. (**D**) Wild-type and the indicated mutants of FLAG-HERC1 were transfected into MCF7 cells and solubilized in non-denaturing lysis buffer with 0.01% digitonin. Lysates were immunoblotted for FLAG-HERC1. Wild-type and mutant HERC1 proteins showed comparable expression and solubility, suggesting they are not grossly aggregated or eliminated by cellular quality control. (**E**) Post-nuclear supernatants expressing the proteins in panel D were separated by size on a 5-25% sucrose gradient, and visualised by immunoblotting. The three FLAG-HERC1 proteins show similar fractionation profiles. These spin conditions cause a ~300 kD protein to sediment into fractions 3-5, and a ~500 kD protein to sediment into fractions 5-7. Ribosomal subunits are in the pellet fraction.

References and Notes

1. K. E. Bohnsack, M. T. Bohnsack, Uncovering the assembly pathway of human ribosomes and its emerging links to disease. *EMBO J.* **38**, e100278 (2019). doi:10.15252/embj.2018100278 Medline

2. S. Klinge, J. L. Woolford Jr., Ribosome assembly coming into focus. *Nat. Rev. Mol. Cell Biol.* **20**, 116–131 (2019). doi:10.1038/s41580-018-0078-y Medline

3. A. Rousseau, A. Bertolotti, Regulation of proteasome assembly and activity in health and disease. *Nat. Rev. Mol. Cell Biol.* **19**, 697–712 (2018). doi:10.1038/s41580-018-0040-z Medline

4. J. M. Raser, E. K. O'Shea, Noise in gene expression: Origins, consequences, and control. *Science* **309**, 2010–2013 (2005). doi:10.1126/science.1105891 Medline

5. B. Munsky, G. Neuert, A. van Oudenaarden, Using gene expression noise to understand gene regulation. *Science* **336**, 183–187 (2012). doi:10.1126/science.1216379 Medline

6. J. W. Harper, E. J. Bennett, Proteome complexity and the forces that drive proteome imbalance. *Nature* **537**, 328–338 (2016). doi:10.1038/nature19947 Medline

7. Y.-C. Tang, A. Amon, Gene copy-number alterations: A cost-benefit analysis. *Cell* **152**, 394–405 (2013). doi:10.1016/j.cell.2012.11.043 Medline

8. D. Hanahan, R. A. Weinberg, Hallmarks of cancer: The next generation. *Cell* **144**, 646–674 (2011). doi:10.1016/j.cell.2011.02.013 Medline

9. R. Origa, β-Thalassemia. *Genet. Med.* **19**, 609–619 (2017). Medline

10. C. M. Brennan, L. P. Vaites, J. N. Wells, S. Santaguida, J. A. Paulo, Z. Storchova, J. W. Harper, J. A. Marsh, A. Amon, Protein aggregation mediates stoichiometry of protein complexes in aneuploid cells. *Genes Dev.* **33**, 1031–1047 (2019). doi:10.1101/gad.327494.119 Medline

11. N. Dephoure, S. Hwang, C. O'Sullivan, S. E. Dodgson, S. P. Gygi, A. Amon, E. M. Torres, Quantitative proteomic analysis reveals posttranslational responses to aneuploidy in yeast. *eLife* **3**, e03023 (2014). doi:10.7554/eLife.03023 Medline

12. E. M. Torres, T. Sokolsky, C. M. Tucker, L. Y. Chan, M. Boselli, M. J. Dunham, A. Amon, Effects of aneuploidy on cellular physiology and cell division in haploid yeast. *Science* **317**, 916–924 (2007). doi:10.1126/science.1142210 Medline

13. B. R. Williams, V. R. Prabhu, K. E. Hunter, C. M. Glazier, C. A. Whittaker, D. E. Housman, A. Amon, Aneuploidy affects proliferation and spontaneous immortalization in mammalian cells. *Science* **322**, 703–709 (2008). doi:10.1126/science.1160058 Medline

14. D. C. Dieterich, A. J. Link, J. Graumann, D. A. Tirrell, E. M. Schuman, Selective identification of newly synthesized proteins in mammalian cells using bioorthogonal noncanonical amino acid tagging (BONCAT). *Proc. Natl. Acad. Sci. U.S.A.* **103**, 9482–9487 (2006). doi:10.1073/pnas.0601637103 Medline

15. E. McShane, C. Sin, H. Zauber, J. N. Wells, N. Donnelly, X. Wang, J. Hou, W. Chen, Z. Storchova, J. A. Marsh, A. Valleriani, M. Selbach, Kinetic analysis of protein stability

reveals age-dependent degradation. *Cell* **167**, 803–815.e21 (2016). doi:10.1016/j.cell.2016.09.015 Medline

16. C. C. Thoreen, L. Chantranupong, H. R. Keys, T. Wang, N. S. Gray, D. M. Sabatini, A unifying model for mTORC1-mediated regulation of mRNA translation. *Nature* **485**, 109–113 (2012). doi:10.1038/nature11083 Medline

17. M. Ghandi, F. W. Huang, J. Jané-Valbuena, G. V. Kryukov, C. C. Lo, E. R. McDonald 3rd, J. Barretina, E. T. Gelfand, C. M. Bielski, H. Li, K. Hu, A. Y. Andreev-Drakhlin, J. Kim, J. M. Hess, B. J. Haas, F. Aguet, B. A. Weir, M. V. Rothberg, B. R. Paolella, M. S. Lawrence, R. Akbani, Y. Lu, H. L. Tiv, P. C. Gokhale, A. de Weck, A. A. Mansour, C. Oh, J. Shih, K. Hadi, Y. Rosen, J. Bistline, K. Venkatesan, A. Reddy, D. Sonkin, M. Liu, J. Lehar, J. M. Korn, D. A. Porter, M. D. Jones, J. Golji, G. Caponigro, J. E. Taylor, C. M. Dunning, A. L. Creech, A. C. Warren, J. M. McFarland, M. Zamanighomi, A. Kauffmann, N. Stransky, M. Imielinski, Y. E. Maruvka, A. D. Cherniack, A. Tsherniak, F. Vazquez, J. D. Jaffe, A. A. Lane, D. M. Weinstock, C. M. Johannessen, M. P. Morrissey, F. Stegmeier, R. Schlegel, W. C. Hahn, G. Getz, G. B. Mills, J. S. Boehm, T. R. Golub, L. A. Garraway, W. R. Sellers, Next-generation characterization of the Cancer Cell Line Encyclopedia. *Nature* **569**, 503–508 (2019). doi:10.1038/s41586-019-1186-3 Medline

18. N. J. Cowan, Mammalian cytosolic chaperonin. *Methods Enzymol.* **290**, 230–241 (1998). doi:10.1016/S0076-6879(98)90022-2 Medline

19. J. Driscoll, A. L. Goldberg, The proteasome (multicatalytic protease) is a component of the 1500-kDa proteolytic complex which degrades ubiquitin-conjugated proteins. *J. Biol. Chem.* **265**, 4789–4792 (1990). doi:10.1016/S0021-9258(19)34041-4 Medline

20. M. Funakoshi, R. J. Tomko Jr., H. Kobayashi, M. Hochstrasser, Multiple assembly chaperones govern biogenesis of the proteasome regulatory particle base. *Cell* **137**, 887–899 (2009). doi:10.1016/j.cell.2009.04.061 Medline

21. T. Kaneko, J. Hamazaki, S. Iemura, K. Sasaki, K. Furuyama, T. Natsume, K. Tanaka, S. Murata, Assembly pathway of the mammalian proteasome base subcomplex is mediated by multiple specific chaperones. *Cell* **137**, 914–925 (2009). doi:10.1016/j.cell.2009.05.008 Medline

22. J. Roelofs, S. Park, W. Haas, G. Tian, F. E. McAllister, Y. Huo, B.-H. Lee, F. Zhang, Y. Shi, S. P. Gygi, D. Finley, Chaperone-mediated pathway of proteasome regulatory particle assembly. *Nature* **459**, 861–865 (2009). doi:10.1038/nature08063 Medline

23. Y. Saeki, A. Toh-E, T. Kudo, H. Kawamura, K. Tanaka, Multiple proteasome-interacting proteins assist the assembly of the yeast 19S regulatory particle. *Cell* **137**, 900–913 (2009). doi:10.1016/j.cell.2009.05.005 Medline

24. E. Itakura, E. Zavodszky, S. Shao, M. L. Wohlever, R. J. Keenan, R. S. Hegde, Ubiquilins chaperone and triage mitochondrial membrane proteins for degradation. *Mol. Cell* **63**, 21–33 (2016). doi:10.1016/j.molcel.2016.05.020 Medline

25. S. Park, J. Roelofs, W. Kim, J. Robert, M. Schmidt, S. P. Gygi, D. Finley, Hexameric assembly of the proteasomal ATPases is templated through their C termini. *Nature* **459**, 866–870 (2009). doi:10.1038/nature08065 Medline

26. S. Shao, R. S. Hegde, A calmodulin-dependent translocation pathway for small secretory proteins. *Cell* **147**, 1576–1588 (2011). doi:10.1016/j.cell.2011.11.048 Medline

27. S. Shao, R. S. Hegde, Target selection during protein quality control. *Trends Biochem. Sci.* **41**, 124–137 (2016). doi:10.1016/j.tibs.2015.10.007 Medline

28. S. Wickner, M. R. Maurizi, S. Gottesman, Posttranslational quality control: Folding, refolding, and degrading proteins. *Science* **286**, 1888–1893 (1999). doi:10.1126/science.286.5446.1888 Medline

29. D. N. Itzhak, S. Tyanova, J. Cox, G. H. Borner, Global, quantitative and dynamic mapping of protein subcellular localization. *eLife* **5**, e16950 (2016). doi:10.7554/eLife.16950 Medline

30. N. A. Kulak, G. Pichler, I. Paron, N. Nagaraj, M. Mann, Minimal, encapsulated proteomic-sample processing applied to copy-number estimation in eukaryotic cells. *Nat. Methods* **11**, 319–324 (2014). doi:10.1038/nmeth.2834 Medline

31. S. Konermann, M. D. Brigham, A. E. Trevino, J. Joung, O. O. Abudayyeh, C. Barcena, P. D. Hsu, N. Habib, J. S. Gootenberg, H. Nishimasu, O. Nureki, F. Zhang, Genome-scale transcriptional activation by an engineered CRISPR-Cas9 complex. *Nature* **517**, 583–588 (2015). doi:10.1038/nature14136 Medline

32. T. Mashimo, O. Hadjebi, F. Amair-Pinedo, T. Tsurumi, F. Langa, T. Serikawa, C. Sotelo, J.-L. Guénet, J. L. Rosa, Progressive Purkinje cell degeneration in tambaleante mutant mice is a consequence of a missense mutation in HERC1 E3 ubiquitin ligase. *PLOS Genet.* **5**, e1000784 (2009). doi:10.1371/journal.pgen.1000784 Medline

33. R. Ruiz, E. M. Pérez-Villegas, S. Bachiller, J. L. Rosa, J. A. Armengol, HERC 1 ubiquitin ligase mutation affects neocortical, CA3 hippocampal and spinal cord projection neurons: An ultrastructural study. *Front. Neuroanat.* **10**, 42 (2016). doi:10.3389/fnana.2016.00042 Medline

34. T. Hara, K. Nakamura, M. Matsui, A. Yamamoto, Y. Nakahara, R. Suzuki-Migishima, M. Yokoyama, K. Mishima, I. Saito, H. Okano, N. Mizushima, Suppression of basal autophagy in neural cells causes neurodegenerative disease in mice. *Nature* **441**, 885–889 (2006). doi:10.1038/nature04724 Medline

35. L. Zhao, C. Longo-Guess, B. S. Harris, J.-W. Lee, S. L. Ackerman, Protein accumulation and neurodegeneration in the woozy mutant mouse is caused by disruption of SIL1, a cochaperone of BiP. *Nat. Genet.* **37**, 974–979 (2005). doi:10.1038/ng1620 Medline

36. J. W. Lee, K. Beebe, L. A. Nangle, J. Jang, C. M. Longo-Guess, S. A. Cook, M. T. Davisson, J. P. Sundberg, P. Schimmel, S. L. Ackerman, Editing-defective tRNA synthetase causes protein misfolding and neurodegeneration. *Nature* **443**, 50–55 (2006). doi:10.1038/nature05096 Medline

37. A. Shemorry, C.-S. Hwang, A. Varshavsky, Control of protein quality and stoichiometries by N-terminal acetylation and the N-end rule pathway. *Mol. Cell* **50**, 540–551 (2013). doi:10.1016/j.molcel.2013.03.018 Medline

38. M.-K. Sung, T. R. Porras-Yakushi, J. M. Reitsma, F. M. Huber, M. J. Sweredoski, A. Hoelz, S. Hess, R. J. Deshaies, A conserved quality-control pathway that mediates degradation

of unassembled ribosomal proteins. *eLife* **5**, e19105 (2016). doi:10.7554/eLife.19105 Medline

39. Y. Xu, D. E. Anderson, Y. Ye, The HECT domain ubiquitin ligase HUWE1 targets unassembled soluble proteins for degradation. *Cell Discov.* **2**, 16040 (2016). doi:10.1038/celldisc.2016.40 Medline

40. K. Yanagitani, S. Juszkiewicz, R. S. Hegde, UBE2O is a quality control factor for orphans of multiprotein complexes. *Science* **357**, 472–475 (2017). doi:10.1126/science.aan0178 Medline

41. J. García-Cano, A. Martinez-Martinez, J. Sala-Gaston, L. Pedrazza, J. L. Rosa, HERCing: Structural and functional relevance of the large HERC ubiquitin ligases. *Front. Physiol.* **10**, 1014 (2019). doi:10.3389/fphys.2019.01014 Medline

42. J. L. Rosa, R. P. Casaroli-Marano, A. J. Buckler, S. Vilaró, M. Barbacid, p619, a giant protein related to the chromosome condensation regulator RCC1, stimulates guanine nucleotide exchange on ARF1 and Rab proteins. *EMBO J.* **15**, 4262–4273 (1996). doi:10.1002/j.1460-2075.1996.tb00801.x Medline

43. S. Aggarwal, A. D. Bhowmik, V. L. Ramprasad, S. Murugan, A. Dalal, A splice site mutation in *HERC1* leads to syndromic intellectual disability with macrocephaly and facial dysmorphism: Further delineation of the phenotypic spectrum. *Am. J. Med. Genet. A.* **170**, 1868–1873 (2016). doi:10.1002/ajmg.a.37654 Medline

44. L. S. Nguyen, T. Schneider, M. Rio, S. Moutton, K. Siquier-Pernet, F. Verny, N. Boddaert, I. Desguerre, A. Munich, J. L. Rosa, V. Cormier-Daire, L. Colleaux, A nonsense variant in *HERC1* is associated with intellectual disability, megalencephaly, thick corpus callosum and cerebellar atrophy. *Eur. J. Hum. Genet.* **24**, 455–458 (2016). doi:10.1038/ejhg.2015.140 Medline

45. O. Ortega-Recalde, O. I. Beltrán, J. M. Gálvez, A. Palma-Montero, C. M. Restrepo, H. E. Mateus, P. Laissue, Biallelic *HERC1* mutations in a syndromic form of overgrowth and intellectual disability. *Clin. Genet.* **88**, e1–e3 (2015). doi:10.1111/cge.12634 Medline

46. G. E. Utine, E. Z. Taşkıran, C. Koşukcu, B. Karaosmanoğlu, N. Güleray, Ö. A. Doğan, P. Ö. Ş. Kiper, K. Boduroğlu, M. Alikaşifoğlu, *HERC1* mutations in idiopathic intellectual disability. *Eur. J. Med. Genet.* **60**, 279–283 (2017). doi:10.1016/j.ejmg.2017.03.007 Medline

47. O. Fasano, D. Birnbaum, L. Edlund, J. Fogh, M. Wigler, New human transforming genes detected by a tumorigenicity assay. *Mol. Cell. Biol.* **4**, 1695–1705 (1984). doi:10.1128/MCB.4.9.1695 Medline

48. A. Sharma, M. Mariappan, S. Appathurai, R. S. Hegde, In vitro dissection of protein translocation into the mammalian endoplasmic reticulum. *Methods Mol. Biol.* **619**, 339–363 (2010). doi:10.1007/978-1-60327-412-8_20 Medline

49. S. Shao, M. C. Rodrigo-Brenni, M. H. Kivlen, R. S. Hegde, Mechanistic basis for a molecular triage reaction. *Science* **355**, 298–302 (2017). doi:10.1126/science.aah6130 Medline

50. Y. Shimizu, T. Ueda, in *Cell-Free Protein Production: Methods and Protocols*, Y. Endo, K. Takai, T. Ueda, Eds. (Methods in Molecular Biology Series, Humana Press, 2010), pp. 11–21.

51. F. A. Ran, P. D. Hsu, J. Wright, V. Agarwala, D. A. Scott, F. Zhang, Genome engineering using the CRISPR-Cas9 system. *Nat. Protoc.* **8**, 2281–2308 (2013). doi:10.1038/nprot.2013.143 Medline

52. J. Cox, M. Mann, MaxQuant enables high peptide identification rates, individualized p.p.b.-range mass accuracies and proteome-wide protein quantification. *Nat. Biotechnol.* **26**, 1367–1372 (2008). doi:10.1038/nbt.1511 Medline

53. DepMap, Broad (2021): DepMap 21Q2 Public, Dataset. Figshare (2021); https://doi.org/10.6084/m9.figshare.14541774.v2.